Monthly Notices
of the
ROYAL ASTRONOMICAL SOCIETY

MNRAS **502,** 1312–1333 (2021)
Advance Access publication 2021 January 20

doi:10.1093/mnras/stab148

Cosmic rays across the star-forming galaxy sequence – I. Cosmic ray pressures and calorimetry

Roland M. Crocker,[1]★ Mark R. Krumholz[1,2] and Todd A. Thompson[3]

[1]*Research School of Astronomy and Astrophysics, Australian National University, Canberra, 2611 ACT, Australia*
[2]*ARC Centre of Excellence for Astronomy in Three Dimensions (ASTRO-3D), Canberra, 2611 ACT, Australia*
[3]*Department of Astronomy and Center for Cosmology and Astro-Particle Physics, The Ohio State University, Columbus, OH 43210, USA*

Accepted 2021 January 12. Received 2021 January 10; in original form 2020 June 29

ABSTRACT

In the Milky Way (MW), cosmic rays (CRs) are dynamically important in the interstellar medium (ISM), contribute to hydrostatic balance, and may help regulate star formation. However, we know far less about the importance of CRs in galaxies whose gas content or star formation rate (SFR) differ significantly from those of the MW. Here, we construct self-consistent models for hadronic CR transport, losses, and contribution to pressure balance as a function of galaxy properties, covering a broad range of parameters from dwarfs to extreme starbursts. While the CR energy density increases from $\sim$1 eV cm^{-3} to $\sim$1 keV cm^{-3} over the range from sub-MW dwarfs to bright starbursts, strong hadronic losses render CRs increasingly unimportant dynamically as the SFR surface density increases. In MW-like systems, CR pressure is typically comparable to turbulent gas and magnetic pressure at the galactic mid-plane, but the ratio of CR to gas pressure drops to $\sim$10^{-3} in dense starbursts. Galaxies also become increasingly CR calorimetric and gamma-ray bright in this limit. The degree of calorimetry at fixed galaxy properties is sensitive to the assumed model for CR transport, and in particular to the time CRs spend interacting with neutral ISM, where they undergo strong streaming losses. We also find that in some regimes of parameter space hydrostatic equilibrium discs cannot exist, and in Paper II of this series we use this result to derive a critical surface in the plane of star formation surface density and gas surface density beyond which CRs may drive large-scale galactic winds.

Key words: hydrodynamics – instabilities – radiative transfer – cosmic rays – ISM: jets and outflows – galaxies: ISM.

1 INTRODUCTION

Star formation is a remarkably inefficient process: even in the cold, molecular phase of the interstellar medium (ISM), where thermal pressure support is negligible, only $\sim$ 1 per cent of the gas mass converts to stars per free-fall time-scale (e.g. Krumholz & Tan 2007; Krumholz, Dekel & McKee 2012; Leroy et al. 2017; Utomo et al. 2018), or $\sim$ 10 per cent per galactic orbit (e.g. Kennicutt 1998; Kennicutt & Evans 2012). The origin of this inefficiency has long been debated, but it must at least in part be related to the various sources of non-thermal pressure that prevent the ISM from undergoing a catastrophic free-fall collapse to the galactic mid-plane. The most obvious inhibitor of collapse is the supersonic turbulent motions that are ubiquitous in the interstellar media of all observed galaxies. Turbulence may, in turn, be driven either by mechanical feedback from supernovae (SNe), gravitational instabilities as matter flows inward through galaxies, or some combination of both (e.g. Thompson, Quataert & Murray 2005; Ostriker & Shetty 2011; Faucher-Giguère, Quataert & Hopkins 2013; Krumholz & Burkhart 2016; Hayward & Hopkins 2017; Krumholz et al. 2018). Turbulence, moreover, naturally gives rise to a magnetic field that provides a pressure comparable to the turbulent ram pressure (e.g. Federrath et al. 2014; Federrath 2016). However, in the Solar neighbourhood within the Milky Way (MW), the mid-plane pressure contributed by gas motions and magnetic fields is not entirely dominant. Instead, two other sources of non-thermal pressure – radiation and cosmic rays (CRs) – make comparable contributions (Parker 1966; Boulares & Cox 1990).

While we can measure the strength of these non-thermal contributions *in situ* in the Solar neighbourhood, our knowledge of their importance in galaxies with significantly different large-scale properties (e.g. higher or lower surface densities of gas), or even elsewhere in our own Galaxy, is much more indirect and model-based. There has been significant recent theoretical progress on the importance of radiation pressure, but its role in driving turbulence and outflows in both intensely star-forming galaxies and the star clusters of normal galaxies remains uncertain (e.g. Thompson et al. 2005; Andrews & Thompson 2011; Krumholz & Thompson 2012, 2013; Davis et al. 2014; Skinner & Ostriker 2015; Tsang & Milosavljević 2015, 2018; Thompson & Krumholz 2016; Raskutti, Ostriker & Skinner 2016, 2017; Crocker et al. 2018a, b; Wibking, Thompson & Krumholz 2018).

The dynamical importance of CRs is even more uncertain. This is in part because most early work on this question focused only on galactic conditions similar to those found locally (Jokipii 1976; Badhwar & Stephens 1977; Ghosh & Ptuskin 1983; Chevalier & Fransson 1984; Boulares & Cox 1990; Ko, Dougherty & McKenzie 1991; Ptuskin 2001), and/or focused largely on the question of how and whether CRs can drive galactic winds originating in the ionized,

★ E-mail: roland.crocker@anu.edu.au

low-density medium found several scale heights above galactic planes (Ipavich 1975; Breitschwerdt, McKenzie & Voelk 1991; Zirakashvili et al. 1996; Ptuskin et al. 1997; Zirakashvili & Völk 2006; however, for an exception see Breitschwerdt, McKenzie & Voelk 1993). More recent numerical and analytic models have continued in this vein (e.g. Everett et al. 2008; Jubelgas et al. 2008; Samui, Subramanian & Srianand 2010; Wadepuhl & Springel 2011; Uhlig et al. 2012; Booth et al. 2013; Pakmor et al. 2016; Simpson et al. 2016; Recchia, Blasi & Morlino 2016, 2017; Ruszkowski, Yang & Zweibel 2017; Pfrommer et al. 2017; Buck et al. 2019), rather than address the question of whether CRs represent a significant contribution to the support of the neutral material that dominates the total mass budget and occupies at least ~ 50 per cent of the volume (e.g. Dekel et al. 2019) near the mid-plane. Indeed, the vast majority of published simulations that include CR transport do not resolve the neutral phase or galactic scale heights ($\sim$100 pc), and those that do (e.g. Hanasz et al. 2013; Salem & Bryan 2014; Salem, Bryan & Corlies 2016; Chan et al. 2019) generally assume that CR transport in the neutral ISM is identical to that in the ionized ISM (though see Farber et al. 2018), an assumption that is almost certainly incorrect (e.g. Zweibel 2017; Xu & Lazarian 2017; Krumholz et al. 2020). Only a few published models attempt to address the question of CR pressure support in the neutral ISM for non-Solar neighbourhood (mostly starburst or Galactic Centre) conditions (e.g. Thompson et al. 2006; Socrates, Davis & Ramirez-Ruiz 2008; Lacki, Thompson & Quataert 2010; Lacki et al. 2011; Crocker et al. 2011; Crocker 2012; Lacki 2013; Yoast-Hull, Gallagher & Zweibel 2016; Yoast-Hull & Murray 2019; Krumholz et al. 2020).

Observations can provide some insight into the importance of CRs beyond the MW, but thus far those efforts too have proven limited. The well-known far-infrared (IR)–radio correlation (Condon 1992) indicates a correlation between galaxies' star formation rates (SFRs) and their leptonic CR populations, but since synchrotron luminosity depends not just on CR electron acceleration, but on complex factors such as the amplitude of the magnetic field and the local interstellar radiation field, it has proven challenging to draw strong conclusions about CR acceleration from radio observations alone. Several authors have argued that radio observations favour a model in which CR pressure is dynamically weak, but to date all published models have treated the ISM in a simple one-zone approximation through which CR transport is described solely by parametrized time-scales for escape and energy loss (cf. Thompson et al. 2006; Lacki et al. 2010; Lacki 2013). Moreover, radio observations directly constrain only leptonic CRs, whereas hadronic CRs (i.e. protons and heavier ions) carry the bulk of the CR energy density and pressure. Beyond the MW, direct detection of γ-rays produced by the hadronic CRs that carry most of the energy has only recently become possible with the launch of the *Fermi*-Large Area Telescope (*Fermi*-LAT) experiment and the development of the current generation of Imaging Air Cherenkov telescope arrays (e.g. Funk 2015). While there is now an established literature – first anticipating, more recently, contemplating (e.g. Suchkov, Allen & Heckman 1993; Völk, Aharonian & Breitschwerdt 1996; Zirakashvili et al. 1996; Torres et al. 2004; Domingo-Santamaría & Torres 2005; Thompson, Quataert & Waxman 2007; Persic, Rephaeli & Arieli 2008; Lacki et al. 2011; Martin 2014; Yoast-Hull et al. 2016; Pfrommer et al. 2017; Sudoh, Totani & Kawanaka 2018; Peretti et al. 2019) – the implications of the γ-ray detection of star-forming galaxies, the number of star-forming galaxies detected thus far is still $<$10 (e.g. VERITAS Collaboration et al. 2009; Acero et al. 2009; Abdo et al. 2010; Fermi-LAT collaboration 2012, 2019; Martin 2014; Rojas-Bravo & Araya 2016; Ajello et al. 2020; Xi et al. 2020), and such γ-rays signals as have been detected may, in any case, be polluted by contributions from various sources or processes other than a galaxy's diffuse, hadronic CR population.[1]

This summary of the current state of affairs suggests that a first-principles effort to understand where and when CRs might be important, taking into account all the available observational constraints, seems warranted, and this is the primary goal of this paper. We seek to cut a broad swathe across the parameter space of star-forming galaxies, and determine where within this parameter space CRs might be dynamically significant. In a companion paper (Crocker et al. 2020, hereafter Paper II), we use the framework developed here to address the closely related question: When can we expect CRs to start driving winds in the neutral interstellar media of galaxies?

The remainder of this paper is structured as follows: in Section 2 we present the mathematical setup of our problem and, in particular, set out the ordinary differential equation (ODE) system that describes a self-gravitating gaseous disc that maintains a quasi-hydrostatic equilibrium while subject to a flux of CRs injected at its mid-plane; in Section 3 we present, describe, and evaluate the numerical solutions of our ODEs; in Section 4 we consider the astrophysical implications of our findings for CR feedback on the dense, star-forming gas phase of spiral galaxies; and we further discuss our results and summarize in Section 5.

2 SETUP

2.1 Physical model

The physical system that we consider here is similar to that in Breitschwerdt et al. (1991, 1993) and Socrates et al. (2008), and which we have used in previous studies of radiation pressure feedback (Krumholz & Thompson 2012, 2013; Crocker et al. 2018a, b; Wibking et al. 2018): an idealized 1D representation of a portion of a galactic disc consisting of a gas column confined by gravity through which radiation or CRs are forced from below. We are interested in exploring the equilibrium state of such a system with the goal of determining under what circumstances we expect CRs to be a significant contributor to the vertical pressure support of galactic discs. In the companion paper (Paper II), we determine the circumstance under which it is possible for CRs to launch winds of material out of galactic discs. For convenience, we summarize the meanings and definitions of all symbols we introduce in this discussion in Table 1.

2.1.1 *Equations for transport and momentum balance*

We work in 1D, z, the height above the mid-plane,[2] and treat CRs in the fluid dynamical limit whereby they behave as a fluid of given adiabatic index γ_c; below we adopt the relativistic limit and set $\gamma_c = 4/3$. CRs are injected by SN explosions, which we approximate as occurring solely in a thin layer near $z = 0$. Adopting, for example, equation (30) from Zweibel (2017, also cf. McKenzie & Voelk 1982; Breitschwerdt et al. 1993, equation 5) to 1D ($\nabla \rightarrow \mathrm{d}/\mathrm{d}z$) and assuming

[1]Possible contaminants include individual SNRs and/or leptonic γ-ray emission via inverse Compton or bremsstrahlung emission. Emission from AGN may also contribute in some local γ-ray detected galaxies, for example, NGC 1068, NGC 2403, NGC 3424, NGC 4945, and Circinus (e.g. Ajello et al. 2020).

[2]By symmetry, we can just treat the half-plane from vertical height $z = 0$ to $z \rightarrow \infty$.

Table 1. Symbol definitions.

Symbol	Meaning	Defining equation	Adopted value or range
	Galactic disc parameters		
$\Sigma_{\rm gas}$	Gas surface density		1–$10^{4.5}$ M$_\odot$ pc^{-2}
$\dot{\Sigma}_\star$	Star formation surface density		10^{-4}–10^{3} M$_\odot$ pc^{-2} Myr^{-1}
$f_{\rm gas}$	Disc gas fraction		0–1
σ	Gas velocity dispersion		10–100 km s^{-1}
β	Gas velocity dispersion normalized to c	$\beta = \sigma/c$	3×10^{-5}–3×10^{-4}
χ	Ion mass fraction		10^{-4}–10^{-2}
v_A	Gas Alfvén speed		10–100 km s^{-1}
$\mathcal{M}_A$	Alfvén Mach number	$\mathcal{M}_A = \sigma/v_A$	1.5 (1–2)
ϕ_B	Magnetic support parameter	10	28/27
	CR quantities		
$\kappa_{\rm conv}$	Convective diffusion coefficient	16	
K_*	Mid-plane diffusion coefficient normalized to $\kappa_{\rm conv}$	17	
q	Index of diffusion coefficient–density relation	17	1/4 (1/6–1/2)
$\Sigma_{\rm pp}$	Grammage required to reduce CR flux by one e-folding	28	1.6×10^5 M$_\odot$ pc^{-2}
$\tau_{\rm pp}$	Ratio of $\Sigma_{\rm gas}$ to $\Sigma_{\rm pp}$	29	
v_s	CR streaming speed	41	
β_s	CR streaming speed normalized to c	$\beta_s = v_s/c$	
$\epsilon_\star$	CR energy injected per unit mass of star formation	71	5.6×10^{47} erg M$_\odot^{-1}$
	Scaling factors		
$\Sigma_{\rm gas,\,1}$	$\Sigma_{\rm gas,\,1} = \Sigma_{\rm gas}/10$ M$_\odot$ pc^{-2}		0.1–$10^{3.5}$
$\dot{\Sigma}_{\star,2}$	$\dot{\Sigma}_{\star,2} = \dot{\Sigma}_\star/10^2$ M$_\odot$ pc^{-2} Myr^{-1}		10^2–10^5
σ_1	$\sigma_1 = \sigma/10$ km s^{-1}		1–10
χ_{-4}	$\chi_{-4} = \chi/10^{-4}$		1–100
	Reference (normalizing) quantities		
z_*	Scale height	18	
g_*	Gravitational acceleration	19	
ρ_*	Density	20	
P_*	Pressure	21	
	Dimensionless model quantities		
ξ	Height above mid-plane	23	
s	Column density from mid-plane	23	
p_c	CR pressure	23	
$\mathcal{F}_c$	CR flux	23	
r	Gas density	$r = {\rm d}s/{\rm d}\xi$	
$\tau_{\rm stream}$	Optical depth of disc to CR streaming losses	31	
$\tau_{\rm abs}$	Optical depth of disc to CR absorption losses	31	

a stationary configuration ($\partial X/\partial t \to 0$ and $v_{\rm gas} \to 0$), but also now accounting for collisional energy losses of CRs (not included in the equation written down by Zweibel 2017) we have the following equation for CR transport:

$$\frac{{\rm d}F_c}{{\rm d}z} = -\frac{u_c}{t_{\rm col}} + v_s\frac{{\rm d}P_c}{{\rm d}z}\,, \tag{1}$$

in which $F_c = F_c(z)$ is the CR energy flux,[3] $u_c = u_c(z)$ is the CR energy density, $P_c = P_c(z) = (\gamma_c - 1)u_c$ is the CR pressure, $t_{\rm col}$ is the time-scale for collisional losses, and the final term on the RHS of equation (1) describes exchange of energy between CRs and magnetic waves mediated by the streaming instability. Here, v_s is the CR streaming speed, which depends on the microphysical CR transport mechanism; we defer the question of its value for the moment, and for now simply treat it as a known quantity. We also omit second-order *Fermi* acceleration, on the grounds that it is likely unimportant compared to CR escape and collisional losses (Zweibel 2017). In keeping with our assumption that all CR injection happens at $z = 0$, we do not include a source term in equation (1); instead, we adopt a boundary condition that F_c takes on some particular non-zero value at $z = 0$.

The (quasi-)hydrostatic equilibrium condition gives us a second ODE[4]:

$$\frac{\rm d}{{\rm d}z}\left(P_c + P_{\rm gas} + P_B - 2P_{B_z}\right) = -\rho_{\rm gas}g_z \tag{2}$$

Here, $P_{\rm gas}$ is the gas pressure, $P_B = |\boldsymbol{B}|^2/(8\pi)$ is the total magnetic field pressure,[5] $-2\,{\rm d}P_{B_z}/{\rm d}z = -(1/4\pi){\rm d}(|B_z|^2)/{\rm d}z$ is the magnetic tension force in the vertical direction, $\rho_{\rm gas} = \rho_{\rm gas}(z)$ is the volumetric

[3]Note that, in full generality, the CR energy flux contains both diffusive and advective contributions. As we explain below, however, here and, in particular, in Crocker, Krumholz & Thompson (2020), we are interested in probing the condition of hydrostatic equilibrium. Thus, the systematic flow of the gas in our model is set to zero. Furthermore, while CRs may still stream with respect to the (quasi) static gas, following Krumholz et al. (2020) we shall actually treat this motion via an effective diffusion coefficient. Altogether, these mean that below, the CR flux shall contain only a diffusive part: see equation (14).

[4]Note that the magnetic waves launched by CR streaming provide, in principle, a yet further pressure term (cf. Ko et al. 1991). However, given that our primary interest below is in the physical regime where ion-neutral damping quickly kills such waves, we approximate their pressure contribution as zero.

[5]Note that, while it is the *total* magnetic field that appears, in principle, in the equation of hydrostatic balance (see Boulares & Cox 1990 and also

gas density, and

$$g_z(z) = 4\pi G \left[\Sigma_{\mathrm{gas},1/2}(z) + \Sigma_{\star,1/2}(z)\right]. \quad (3)$$

is the magnitude of the acceleration in the vertical direction. This acceleration is due to a combination of stars and gas; the gas half-column integrated from the mid-plane to any height z is

$$\Sigma_{\mathrm{gas},1/2}(z) = \int_0^z \rho_{\mathrm{gas}}(z')\,\mathrm{d}z', \quad (4)$$

while the stellar half-column is $\Sigma_{\star,\,1/2}$. Consistent with our treatment of CR injection, we assume the stars are in a thin layer near $z = 0$, so $\Sigma_{\star,\,1/2}$ is constant for all $z > 0$. The total column of gas through the disc, i.e. including both $z < 0$ and $z > 0$, we denote (without the z argument) as

$$\Sigma_{\mathrm{gas}} = \lim_{z\to\infty} 2\Sigma_{\mathrm{gas},1/2}(z) \quad (5)$$

and the total stellar column is $\Sigma_\star = 2\Sigma_{\star,\,1/2}$. For future convenience, we also define the total gas fraction

$$f_{\mathrm{gas}} = \frac{\Sigma_{\mathrm{gas}}}{\Sigma_{\mathrm{gas}} + \Sigma_\star}, \quad (6)$$

so the total surface mass density is

$$\Sigma_{\mathrm{tot}} = \frac{\Sigma_{\mathrm{gas}}}{f_{\mathrm{gas}}}. \quad (7)$$

The next step in our calculation is to adopt models for the various terms appearing in equations (1) and (2); we proceed to do so in the remainder of this section.

2.1.2 *Model for gas and magnetic pressure*

Essentially all observed galaxies have neutral gas velocity dispersions that are at least trans-sonic (e.g. Stilp et al. 2013; Ianjamasimanana et al. 2015; Caldú-Primo et al. 2015; for a recent compilation, see Krumholz et al. 2018), so that turbulent pressure support is as or more important than thermal pressure. We must therefore adopt a model for turbulence. Given that this turbulence is injected at scales approaching the gas scale height and cascades down from there, we shall make the assumption that the turbulent velocity dispersion σ of the gas is constant. This position-independent turbulent velocity dispersion together with the local matter density sets the dynamical pressure within the gas column:

$$P_{\mathrm{gas}}(z) = \frac{2}{3}u_{\mathrm{turb}}(z) = \rho_{\mathrm{gas}}(z)\sigma^2, \quad (8)$$

where u_{turb} is the turbulent energy density and $\sigma^2 = \mathrm{const}$ is the turbulent velocity dispersion.

We further assume that the ratio of magnetic to turbulent energy is roughly constant, as expected for a magnetic field that is largely the product of a turbulent dynamo (e.g. Ostriker, Stone & Gammie 2001; Federrath et al. 2014; Federrath 2016). Under this assumption, we can rewrite equation (2) as

$$\frac{\mathrm{d}P_c}{\mathrm{d}z} + \phi_{\mathrm{B}}\sigma^2\frac{\mathrm{d}\rho_{\mathrm{gas}}}{\mathrm{d}z} = -\rho_{\mathrm{gas}}g_z, \quad (9)$$

where

$$\phi_{\mathrm{B}} \equiv 1 + \frac{P_B - 2P_{B_z}}{P_{\mathrm{gas}}}. \quad (10)$$

The quantity ϕ_{B} lies in the range 0–2, with values >1 indicating magnetic pressure support and values <1 indicating confinement by magnetic tension. If the turbulence is isotropic (i.e. $B_z^2 \simeq |\boldsymbol{B}|^2/3$), then the action of the turbulent dynamo is expected to amplify the local magnetic field amplitude such that it is close to, but perhaps slightly below, equipartition with respect to the energy density of the gas turbulent motions (Federrath 2016); this implies that we have strictly $\mathcal{M}_{\mathrm{A}} \geq 1$ with an expected value of $\mathcal{M}_{\mathrm{A}}$ in the range ∼1–2 (see Federrath 2016; Krumholz et al. 2020). Given this we have that ϕ_B is further restricted to the small range 1–13/12. We henceforth adopt $\mathcal{M}_{\mathrm{A}} = 1.5$ and the resultant $\phi_{\mathrm{B}} = 28/27$ as our fiducial choices for these parameters.

2.1.3 *Model for CR collisional losses*

The collisional loss time-scale is

$$t_{\mathrm{col}}(z) = \frac{1}{cn(z)\sigma_{\mathrm{col}}\eta_{\mathrm{col}}} \quad (11)$$

in which $n(z)$ is the position-dependent target nucleon density, and σ_{col} and η_{col} are the total cross-section and inelasticity of the relevant collisional loss process. Given that relativistic ions dominate the energy density for reasonable assumptions about the CR distribution,[6] and consistent with our earlier choice to set $\gamma_c \to 4/3$, we shall ignore the energetically subdominant, low-energy, subrelativistic CR population, and treat the CRs in the relativistic limit. Given the relativistic CRs are close to or above the pion production threshold, we shall consequently assume that CR collisional losses are dominated by hadronic processes (rather than Coulomb or ionizing collisions which dominate for subrelativistic CR ions). In this case for the cross-section and elasticity σ_{col} and η_{col} in equation (11) we have (e.g. Kafexhiu et al. 2014)

$$\sigma_{\mathrm{col}} \to \sigma_{\mathrm{pp}} \simeq 40\ \mathrm{mbarn\ and}\ \eta_{\mathrm{col}} \to \eta_{\mathrm{pp}} \simeq 1/2. \quad (12)$$

Note that the hadronic collision cross-section is only weakly energy dependent above CR (proton) kinetic energies of $T_c \sim$ GeV; given that CR protons are expected to dominate the 'target' and 'beam' populations, we generically label these as 'pp', and we set the target density to $n(z) = \rho_{\mathrm{gas}}(z)/\mu_p m_p$, where m_p is the proton mass and $\mu_p \simeq 1.17$ is the ratio of protons to total nucleons for a gas that is 90 per cent H and 10 per cent He by number. For these choices, the collisional loss time-scale is

$$t_{\mathrm{col}} = 53n_0^{-1}\ \mathrm{Myr} = 100\rho_{\mathrm{gas},-24}^{-1}\ \mathrm{Myr}, \quad (13)$$

where $n_0 = n/1\ \mathrm{cm}^{-3}$ and $\rho_{\mathrm{gas},\,-24} = \rho_{\mathrm{gas}}/10^{-24}\ \mathrm{g\,cm}^{-3}$.

2.1.4 *CR fluxes*

The final model we must adopt is a description of how CRs interact with the magnetized turbulence in the ISM, which in turn will specify the CR flux, F_c. The microphysical processes responsible for scattering and confining CRs are significantly uncertain, and for this reason we will leave our analysis as generic as possible for the

section 10.1.2 of Krumholz 2015), below we shall specialize to the physically plausible case where the turbulent magnetic field is dominant.

[6]Specifically, we assume that the ions follow a power-law distribution in (the absolute magnitude of the) momentum (Bell 1978), p, falling somewhat more steeply than p^{-2} as a result of first-order *Fermi* acceleration in combination with transport time-scales that also decline with momentum. CR electrons, which suffer considerably more severe losses than ions, are expected (e.g. Strong et al. 2010) to constitute $\lesssim$ few per cent of the total CR energy density for ISM conditions in star-forming galaxies.

moment, deferring detailed models to Section 2.3. We treat the flux in the standard diffusion approximation (Ginzburg & Syrovatskii 1964), whereby

$$F_c = -\kappa \frac{\mathrm{d}u_c}{\mathrm{d}z}. \tag{14}$$

It is convenient to normalize κ to its minimum possible value, by writing

$$\kappa = K\kappa_{\rm conv}, \tag{15}$$

where

$$\kappa_{\rm conv} = \frac{z_*\sigma}{3} = \frac{\sigma^3 f_{\rm gas}}{6\pi\, G\, \Sigma_{\rm gas}} \simeq 3.8\times 10^{26}\ \mathrm{cm^2\ s^{-1}}\ \sigma_1^3\ f_{\rm gas}\ \Sigma_{\rm gas,1}^{-1}, \tag{16}$$

z_* is the gas scale height (defined precisely below), and we have defined $\sigma_1 = \sigma/10\ \mathrm{km\ s^{-1}}$ and $\Sigma_1 = \Sigma_{\rm gas}/(10\ \mathrm{M_\odot\ pc^2})$; the velocity dispersion and gas surface density to which we have scaled are the approximate values in the Solar neighbourhood. Here, $\kappa_{\rm conv}$ is the 'convective' diffusion coefficient that would apply if we were to assume that CRs were perfectly frozen into the gas, and were mixed solely by passive advection along with the gas, which is stirred by turbulence with a characteristic coherence length of order the galactic scale height (Tennekes & Lumley 1972). Since convection occurs in addition to whatever processes might allow CRs to move relative to the gas, the true diffusion coefficient is always greater than the convective one, and thus we have $K \gtrsim 1$.

In addition to the value of K, we must adopt a model for its dependence on density or scale height. This is inextricably linked to the microphysical model of CR propagation that we will discuss below, but for now we note that we generically expect K to rise as the density falls. This is because, as one moves out of the mid-plane of galaxies, magnetic fields become progressively less turbulent, more ordered, and weaker (Beck 2015), presenting less of a barrier to CR propagation. Given the uncertainties of exactly how the disc–halo transition for the magnetic field occurs, we elect to follow Krumholz et al. (2020) by parametrizing our ignorance: we assume that the dimensionless diffusion coefficient K scales with the gas density as

$$K = K_*\left(\frac{\rho_{\rm gas}}{\rho_*}\right)^{-q}, \tag{17}$$

where ρ_* and K_* are normalizing factors that we are free to choose. As we discuss below in the context of our specific CR propagation models, the plausible range for the index q is $q = 1/6$–$1/2$. We will adopt $q = 1/4$ as a fiducial choice; Krumholz et al. (2020) show that the results of CR propagation models are not highly sensitive to this choice, within the plausible physical range.

2.2 Non-dimensionalization

We have now specified models for all terms appearing in the transport and hydrostatic balance equations. Our next step is to non-dimensionalize the equations and, in the process, extract the key dimensionless numbers that govern the system. The natural length-scale for our system is the scale height of the disc imposed by turbulence,

$$z_* = \frac{\sigma^2}{g_*}, \tag{18}$$

where

$$g_* = 2\pi G\frac{\Sigma_{\rm gas}}{f_{\rm gas}} \tag{19}$$

is the characteristic acceleration due to the matter column.[7] The length-scale z_* also immediately defines a characteristic density scale

$$\rho_* = \frac{\Sigma_{\rm gas}}{2z_*} = \frac{\pi G}{f_{\rm gas}}\left(\frac{\Sigma_{\rm gas}}{\sigma}\right)^2, \tag{20}$$

which gives the typical density of gas near the mid-plane.

Other natural scales are the characteristic mid-plane pressure P_* (with related energy density $u_* = (3/2)P_*$) is given by

$$P_* = g_*\rho_* z_* = \rho_*\sigma^2 = \frac{\pi G}{f_{\rm gas}}\Sigma_{\rm gas}^2, \tag{21}$$

and the associated flux required if the pressure is carried by a collection of relativistic particles in the free-streaming limit

$$F_* = cP_* = \frac{\pi G c}{f_{\rm gas}}\Sigma_{\rm gas}^2. \tag{22}$$

We now proceed to non-dimensionalize our system by defining the non-dimensional variables

$$\xi = \frac{z}{z_*}\ s(\xi) = \left.\frac{\Sigma_{\rm gas,1/2}(z)}{\rho_* z_*}\right|_{z=z_*\xi}$$
$$p_c(\xi) = \left.\frac{P_c(z)}{P_*}\right|_{z=z_*\xi}\ \mathcal{F}_c(\xi) = \left.\frac{F_c(z)}{F_*}\right|_{z=z_*\xi}. \tag{23}$$

Here ξ, s, and p_c are the dimensionless height, gas (half) column, CR pressure, and flux; $\mathrm{d}s/\mathrm{d}\xi$ is the dimensionless gas density. The physical density is

$$\rho(z) = \rho_*\left.\frac{\mathrm{d}s}{\mathrm{d}\xi}\right|_{\xi=z/z_*}. \tag{24}$$

Changing to these variables, the CR transport equation (1), becomes

$$\frac{\mathrm{d}\mathcal{F}_c}{\mathrm{d}\xi} = -3\frac{z_*}{ct_{\rm col}}p_c + \beta_s\frac{\mathrm{d}p_c}{\mathrm{d}\xi} \tag{25}$$

where $\beta_s \equiv v_s/c$. Making use of equations (15) and (17), the dimensionless flux is

$$\mathcal{F}_c = -K_*\beta\left(\frac{\mathrm{d}s}{\mathrm{d}\xi}\right)^{-q}\frac{\mathrm{d}p_c}{\mathrm{d}\xi}, \tag{26}$$

where $\beta \equiv \sigma/c$. Similarly non-dimensionalizing the collisional loss term (equation 11), we have

$$\frac{3z_*}{ct_{\rm col}} = \frac{3\eta_{\rm pp}\sigma_{\rm pp}}{\mu_p m_p}\frac{\Sigma_{\rm gas}}{2}\frac{\mathrm{d}s}{\mathrm{d}\xi}. \tag{27}$$

We define

$$\Sigma_{\rm pp} \equiv \frac{\mu_p m_p}{3\eta_{\rm pp}\sigma_{\rm pp}} \simeq \frac{33\ \mathrm{g\ cm^{-2}}}{(\eta_{\rm pp}/0.5)(\sigma_{\rm pp}/40\ \mathrm{mbarn})} \simeq 1.6\times 10^5\ \mathrm{M_\odot\ pc^{-2}} \tag{28}$$

as the grammage required to decrease the CR flux by one e-folding, so that

$$\frac{3z_*}{ct_{\rm col}} = \frac{\Sigma_{\rm gas}}{2\Sigma_{\rm pp}}\frac{\mathrm{d}s}{\mathrm{d}\xi} \equiv \tau_{\rm pp}\frac{\mathrm{d}s}{\mathrm{d}\xi}. \tag{29}$$

Here, $\tau_{\rm pp}$ is the ratio of the gas half-surface density to $\Sigma_{\rm pp}$, which represents the optical depth to absorption that a CR travelling in a

[7] Note that, given our assumption the stars are distributed in a vanishingly thin sheet, this is the scale height of the gas distribution in the limit $f_{\rm gas} \to 0$. In the opposite limit, $f_{\rm gas} \to 1$, the scale height goes to $2z_*$.

straight line out of the galaxy would experience; we will see below that the actual optical depth to escape the galaxy is much larger than this. Inserting the quantities above into equation (25), and with some minor re-arrangement, we arrive at the following form of the dimensionless CR transport equation:

$$\frac{\mathrm{d}}{\mathrm{d}\xi}\left[-\left(\frac{\mathrm{d}s}{\mathrm{d}\xi}\right)^{-q}\frac{\mathrm{d}p_c}{\mathrm{d}\xi}\right] = -\tau_{\mathrm{abs}}\frac{\mathrm{d}s}{\mathrm{d}\xi}p_c + \tau_{\mathrm{stream}}\frac{\mathrm{d}p_c}{\mathrm{d}\xi}, \tag{30}$$

where

$$\tau_{\mathrm{stream}} = \frac{\beta_s}{K_*\beta} = \frac{1}{K_*}\frac{v_s}{\sigma} \tag{31}$$

$$\tau_{\mathrm{abs}} = \frac{\tau_{\mathrm{pp}}}{K_*\beta}. \tag{32}$$

Equation (30) asserts that the change in CR flux with respect to height (the LHS) is equal to the rate at which CRs are lost due to collisions (the first term on the RHS) and dissipation of CR energy into Alfvén waves, and ultimately into thermal energy, via the streaming instability (the second term on the RHS), and we can conceptualize τ_{abs} and τ_{stream} as the 'absorption' and 'streaming' optical depths of the gas column to CRs. As noted above, the effective absorption optical depth τ_{abs} is larger than the optical depth τ_{pp} experienced by a CR travelling in a straight line at c by a factor of $1/K_*\beta \gg 1$. This factor accounts for the fact that, although the effective speed of CRs diffusing out of the disc is $K_*\sigma$, their microphysical speed is still c, so the reduction in effective speed means that grammage they traverse in going a given distance must be increased by a factor $c/K_*\sigma$.

Repeating these procedures for the equation of momentum balance, equation (2), and making use of equation (9), yields the non-dimensionalized equation

$$\frac{\mathrm{d}p_c}{\mathrm{d}\xi} + \phi_{\mathrm{B}}\frac{\mathrm{d}^2 s}{\mathrm{d}\xi^2} = -\left(1 - f_{\mathrm{gas}}\right)\frac{\mathrm{d}s}{\mathrm{d}\xi} - f_{\mathrm{gas}}s\frac{\mathrm{d}s}{\mathrm{d}\xi}. \tag{33}$$

The terms in equation (33) are, from left to right, the pressure gradient due to CRs, the pressure gradient due to combined turbulence plus magnetic support, the gravitational acceleration due to stellar gravity, and the acceleration due to gas self-gravity.

Finally, our system of equations (30) and (33) is fourth order in total, and thus requires four boundary conditions. Two of these are

$$s(0) = 0 \tag{34}$$

$$\lim_{\xi\to\infty} s(\xi) = 1, \tag{35}$$

which amount to asserting that the gas half-column is zero at the mid-plane, and that $\lim_{z\to\infty}\Sigma_{\mathrm{gas},\,1/2}(z) = 1/2\,\Sigma_{\mathrm{gas}}$. For the boundary conditions on the CR pressure, we can re-arrange the dimensionless CR flux, equation (26), and evaluate it at $\xi = 0$. This generates a third boundary condition,

$$-\left(\frac{\mathrm{d}s}{\mathrm{d}\xi}\right)^{-q}\frac{\mathrm{d}p_c}{\mathrm{d}\xi}\bigg|_{\xi=0} = \frac{\tau_{\mathrm{stream}}}{\beta_s}\frac{F_{c,0}}{F_*} \equiv f_{\mathrm{Edd}}, \tag{36}$$

where the quantity f_{Edd} is the ratio of the incoming CR flux to the Eddington flux, defined here as the flux for which the momentum flux carried in the $+z$-direction by the CRs matches the momentum flux in the $-z$-direction due to gravity. Note here that $F_{c,\,0}$ is enhanced by the factor $\tau_{\mathrm{stream}}/\beta_s$ that accounts for the diffusive nature of the CR transport (cf. Socrates et al. 2008).

To obtain the final boundary condition, we follow Krumholz et al. (2020) and demand that the solution of CR propagation within the disc join smoothly to the solution for free-streaming CRs as $z \to \infty$, on the basis that, once one is sufficiently high above the disc, field lines should straighten out and CRs should be able to free-stream to infinity at the Alfvén velocity. This condition requires that the CR enthalpy flux obey

$$\lim_{z\to\infty}\frac{F_c}{u_c + P_c} = v_{s,\infty}, \tag{37}$$

where $v_{s,\,\infty}$ is the streaming speed well above the disc. In terms of the dimensionless parameters, this becomes

$$\lim_{\xi\to\infty}\frac{1}{\tau_{\mathrm{stream},\infty}}\left(\frac{\mathrm{d}s}{\mathrm{d}\xi}\right)^{-q}\frac{\mathrm{d}p_c}{\mathrm{d}\xi} = \lim_{\xi\to\infty} 4\,\mathrm{sign}\left(\frac{\mathrm{d}p_c}{\mathrm{d}\xi}\right)\,p_c(\xi), \tag{38}$$

with $\tau_{\mathrm{stream},\,\infty}$ defined identically to τ_{stream}, but with $v_{s,\,\infty}$ in place of v_s (cf. equation 31). In general we expect $v_{s,\,\infty} > v_s$ and thus $\tau_{\mathrm{stream},\,\infty} > \tau_{\mathrm{stream}}$, because the density falls faster than the magnetic field strength as z increases (though this may be compensated for by increases in the ionization fraction with height – see Section 2.3.1). However, in practice this makes little difference; numerical experimentation shows that varying the ratio $\tau_{\mathrm{stream},\,\infty}/\tau_{\mathrm{stream}}$ over the range 1–100 leads to $\ll 1$ per cent changes in the density and pressure profiles of the resulting solutions. This is not surprising: the choice of $\tau_{\mathrm{stream},\,\infty}$ sets the effective propagation speed of CRs at $z \gg 0$, but as long as this speed is large compared to the effective propagation speed near the mid-plane, which it is for any reasonable choice of $\tau_{\mathrm{stream},\,\infty}/\tau_{\mathrm{stream}}$, the exact numerical value of $\tau_{\mathrm{stream},\,\infty}$ has little effect on the results. For simplicity we will therefore adopt $\tau_{\mathrm{stream},\,\infty} = \tau_{\mathrm{stream}}$ hereafter.

2.3 CR transport models

The values of K and v_s depend on the microphysics of CR confinement, which, as noted above, are substantially uncertain. For this reason, we consider three possible transport models, three based on theory and one purely empirical, that differ in their predicted scalings of κ with large-scale galaxy properties. For convenience, we collect the predicted scalings of various parameters with galaxy properties in Table 2, and we compare the various models in Section 2.3.4.

As presaged above, for any model of CR diffusion, convective transport sets a lower limit to the diffusion coefficient. Moreover, convection is likely to be roughly the correct model for transport if CRs are self-confined by the streaming instability and the medium in which they propagate is mostly ionized. This is because, for CRs with energies ∼1 GeV, the streaming velocity is close to the Alfvén speed even in mostly ionized media (Skilling 1971; Wiener, Pfrommer & Oh 2017). Thus, if the turbulence is Alfvénic or mildly super-Alfvénic, per our dynamo-inspired model, convective transport will in fact dominate.

In this scenario, we trivially have $K_* = 1$ (with the dimensional diffusion coefficient given by equation 16) which implies a maximum escape time through the gas column

$$t_{\mathrm{esc,diff}} = 100 f_{\mathrm{gas}}\frac{\sigma_1}{\Sigma_{\mathrm{gas},1}}\ \mathrm{Myr}. \tag{39}$$

The absorption optical depth for convective transport is

$$\tau_{\mathrm{abs}} = \frac{\tau_{\mathrm{pp}}}{\beta} = 1.1\frac{\Sigma_{\mathrm{gas},1}}{\sigma_1}; \tag{40}$$

this sets an upper limit to the effective τ_{abs} for the transport modes discussed below.

Table 2. Key dimensionless quantities for the four CR propagation models considered in this paper. In this table, M_A is the Alfvén Mach number of the Alfvénic turbulent modes, σ is the gas velocity dispersion, $\beta = \sigma/c$, $\Sigma_{\rm gas}$ is the gas surface density, $f_{\rm gas}$ is the gas fraction, $E_{\rm CR}$ is the CR energy, p is the index of the turbulent magnetic field fluctuation–size relation (1/3 for Kolmogorov and 1/2 for Kraichnan), $\kappa_{*,\rm MW}$ is our fiducial MW diffusion coefficient, and $\tau_{\rm pp}$ is the optical depth of the galactic disc to CRs moving in straight lines at c.

Quantity	CR transport model Streaming (Section 2.3.1)	Scattering (Section 2.3.2)	Constant κ_* (Section 2.3.3)
K_*	$\frac{1}{\sqrt{2\chi}M_A^4}$	$\frac{1}{\beta}\left(\frac{G}{2f_{\rm gas}}\right)^{p/2}\left(\frac{E_{\rm CR}M_A}{e\sigma^2}\right)^{p}$	$\frac{6\pi G\Sigma_{\rm gas}\kappa_{*,\rm MW}}{f_{\rm gas}\sigma^3}$
v_s/σ	$\frac{1}{\sqrt{2\chi}M_A}$	$\frac{1}{\sqrt{2}M_A}$	$\frac{1}{\sqrt{2}M_A}$
$\tau_{\rm stream}$	M_A^3	$\frac{\beta}{\sqrt{2}M_A}\left(\frac{G}{2f_{\rm gas}}\right)^{-p/2}\left(\frac{E_{\rm CR}M_A}{e\sigma^2}\right)^{-p}$	$\frac{f_{\rm gas}\sigma^3}{6\sqrt{2}\pi GM_A\kappa_{*,\rm MW}\Sigma_{\rm gas}}$
$\tau_{\rm abs}$	$\frac{\sqrt{2\chi}M_A^4}{\beta}\tau_{\rm pp}$	$\left(\frac{G}{2f_{\rm gas}}\right)^{-p/2}\left(\frac{E_{\rm CR}M_A}{e\sigma^2}\right)^{-p}\tau_{\rm pp}$	$\frac{f_{\rm gas}\sigma^2 c}{6\pi G\Sigma_{\rm gas}\kappa_{*,\rm MW}}\tau_{\rm pp}$

2.3.1 Streaming plus field line random walk

Our first model, which we will use as our fiducial choice throughout the paper, is that presented by Xu & Lazarian (2017) and Krumholz et al. (2020). We refer readers to those papers for full details, and here simply summarize the most important results. The motivation for this model is that the star-forming part of the ISM, the part that dominates the mass budget and for which we are interested in feedback effects, is neutral rather than ionized; even by volume the neutral material occupies ~ 50 per cent of the available space at the mid-plane (e.g. Dekel et al. 2019), rising to near unity as one goes to more gas-rich and intensely star-forming systems. Thus, even though CRs may spend a significant portion of their lives in the ionized galactic halo (as is observed to be the case in the MW), transport through the neutral ISM that dominates the mass budget is what matters for the purposes of determining whether CRs provide significant pressure support.

In a predominantly neutral medium, strong ion-neutral damping cuts off the turbulent cascade in the ISM, and decouples ions from neutrals, at scales far larger than the gyroradii of ~GeV CRs. Consequently, dissipation of CR energy via streaming instability occurs into Alfvén waves that propagate in the ions alone, and thus have speed

$$v_s = v_{A,i} = \frac{v_A}{\sqrt{\chi}} = \frac{\sigma}{\sqrt{2\chi}M_A} \tag{41}$$

where χ is the ionization fraction by mass, M_A is the Alfvén Mach number of the turbulence in the ISM, and the factor 2 in the denominator of the last term arises from the assumption that Alfvénic modes carry half the turbulent energy. As noted above, dynamo models predict $M_A \simeq 1$–2. We adopt $M_A = 1.5$ as a fiducial choice unless noted otherwise, but explore this dependence below.

Since the external turbulence does not couple to CRs, CR transport in such a medium occurs predominantly by CRs streaming along field lines at the ion Alfvén speed,[8] coupled with the random walk of those field lines in the overall turbulence, implying an effective mean-free path equal to the magnetic field coherence length. The corresponding diffusion coefficient is therefore

$$\kappa = \frac{v_{A,i}l_{\rm coh,B}}{3}, \tag{42}$$

where $l_{\rm coh,\,B}$ is the coherence length of the magnetic field, which for a dynamo-generated field is

$$l_{\rm coh,B} \simeq \frac{z_*}{M_A^3}. \tag{43}$$

Consequently, for this model we adopt

$$K_* = \frac{1}{\sqrt{2\chi}M_A^4} \simeq \frac{22.4}{\chi_{-3}^{1/2}M_A^4} \tag{44}$$

It immediately follows that[9]

$$\tau_{\rm stream} = M_A^3 \tag{45}$$

$$\tau_{\rm abs} = \frac{\sqrt{2\chi}M_A^4}{\beta}\tau_{\rm pp} = 0.043\frac{M_A^4\Sigma_{\rm gas,1}}{\chi_{-3}^{1/2}\sigma_1}, \tag{46}$$

where $\chi_{-3} = \chi/10^{-3}$; the ionization fraction to which we have chosen to normalize is intermediate between the values of $\sim 10^{-4}$ found in starbursts (Krumholz et al. 2020) and the value $\sim 10^{-2}$ found in the warm atomic medium of galaxies like the MW (Wolfire et al. 2003). Thus, $\tau_{\rm abs}$ is somewhat less than unity for MW-like parameters, but becomes larger than unity for galaxies with larger gas surface densities. As discussed in Krumholz et al. (2020), the value of q for this model, which specifies the density scaling, is uncertain because it depends on how the ionization fraction and coherence length of the magnetic field vary with height. However, Krumholz et al.

[8]For CR energies $\gg$ GeV, given a reasonable power-law spectral distribution, the energy density of CRs available to excite magnetic field fluctuations at a given gyroradius scale declines sufficiently that the balance between streaming instability and ion-neutral damping no longer implies a streaming speed that is very close to the Alfvén speed. At this point, the streaming velocity then starts to grow again with energy; see Krumholz et al. (2020). However, in this paper we focus solely on the ~GeV CRs that dominate the CR pressure, and these are essentially always in the regime where the streaming speed is close to the Alfvén speed: see Appendix A. Also note that it is an assumption of the streaming model that the CRs' motion along the field lines will act to transport them down their gradient such that they can excite the streaming instability; given the overall anisotropy of our setup (with the CR sources concentrated in the plane), it is clear that, globally, CRs must move down their gradient by escaping out of the disk. However there may be local instances where the gradient criterion is not satisfied forming 'bottleneck' regions. This effect has been investigated numerically by Wiener, Zweibel & Oh (2013) and Wiener et al. (2017).

[9]Note that, for this streaming case, that the optical depth to *scattering* is given by $z_*/l_{\rm coh,B} = M_A^3$ which is identically equal to $\tau_{\rm stream}$. Thus for $M_A \geq 1$, we are safely in the diffusive regime.

(2020) also show that their results are not terribly sensitive to this choice.

For reference, the corresponding dimensional diffusion coefficient is[10]

$$\kappa_* \simeq 8.5 \times 10^{27} \frac{\sigma_1^3 f_{\rm gas} M_A^{-4}}{\sqrt{\chi_{-3}}\ \Sigma_{\rm gas,1}}\ {\rm cm^2\ s^{-1}}, \tag{47}$$

and the diffusive escape time is

$$t_{\rm esc,diff} = \frac{z_*^2}{2\kappa_*} \simeq 4.9 \frac{M_A^4 f_{\rm gas} \chi_{-3}^{1/2} \sigma_1}{\Sigma_{\rm gas,1}}\ {\rm Myr}. \tag{48}$$

For comparison, note that the collisional loss time-scale (equation 11) is

$$t_{\rm col} = \frac{\mu_p m_p}{c \rho_* \sigma_{\rm col} \eta_{\rm col}} = 110\ f_{\rm gas} \left(\frac{\sigma_1}{\Sigma_{\rm gas,1}}\right)^2\ {\rm Myr}. \tag{49}$$

Thus, for MW-like parameters, the collisional loss time is substantially longer than the diffusive escape time, and most CRs do not produce observable γ-ray emission. However, given the generic dependencies $t_{\rm col} \propto \Sigma_{\rm gas}^{-2}$ and $t_{\rm esc,diff} \propto \Sigma_{\rm gas}^{-1}$, collisional losses will always win out over diffusive escape at sufficiently high gas surface density (for other parameters held fixed). This same point will apply equally to all the models we consider.

It is also interesting to compare these two time-scales to the time-scale for loss of CR energy due to damping via streaming instability. By analogy with $t_{\rm col}$ in equation (25), we can define the characteristic streaming loss time as

$$t_{\rm stream} = \frac{3 z_*}{v_s} = 4.9 \frac{M_A f_{\rm gas} \chi_{-3}^{1/2} \sigma_1}{\Sigma_{\rm gas,1}}\ {\rm Myr} \tag{50}$$

Thus we see that, for the fiducial parameters for this model, in a MW-like galaxy the streaming loss time-scale is comparable to the escape time and much smaller than the collisional loss time. However, this conclusion is very sensitive to the assumed Alfvén Mach number ($t_{\rm esc,diff}/t_{\rm stream} \propto M_A^3$). Moreover, the streaming loss time-scale has the same dependence on $\Sigma_{\rm gas}$ as the escape time-scale, and so collisional losses increase in importance relative to streaming losses as one moves to higher surface density galaxies.

2.3.2 Scattering off extrinsic turbulence

Our second theoretically motivated model is intended to apply in ionized regions. Roughly half the volume at the mid-plane of discs of normal galaxies is ionized, and this fraction rises as one moves into the halo, where CRs spend much of their time. Thus, despite the fact that we are mainly interested in the feedback effects of CRs in the neutral ISM, we must consider the possibility that CR propagation is mainly through the ionized phase, and that the force applied by CRs to the neutral ISM occurs primarily at the neutral-ionized interface. In an ionized gas, the turbulent cascade in the magnetic field does reach down to the CR gyroradius; however, there is a great deal of uncertainty about whether CRs are confined primarily by Alfvén waves that they themselves create via the streaming instability, or primarily by waves cascading from larger scales, or some combination of both (e.g. Zweibel 2017; Blasi 2019, and references therein). If CRs are predominantly self-confined, then the transport mechanism is much the same as for the case of predominantly neutral medium, simply with the ionization fraction $\chi = 1$. On the other hand, if they are confined by scattering off the ambient turbulence in the ISM, then we can compute the resulting diffusion coefficient for highly relativistic CRs, following, for example, Jokipii (1971) or Lacki (2013), as

$$\kappa \simeq \frac{c r_g^p z_*^{1-p}}{3}, \tag{51}$$

where we have assumed that z_* is the outer scale of the turbulence,

$$r_g \simeq \frac{E_{\rm CR}}{2eB}, \tag{52}$$

is the CR gyroradius (assuming a mean sin pitch angle of 1/2), and p depends on the index of the turbulent spectrum: $p = 1/3$ for a Kolmogorov spectrum and $p = 1/2$ for a Kraichnan spectrum. We will adopt $p = 1/2$ as a fiducial choice, and use this value for all numerical evaluations; however, we give results for general p. The factor q that describes the density scaling is $q = p/2$, that is, for our fiducial $p = 1/2$, we have $q = 1/4$, so the diffusion coefficient decreases with density as $\kappa \propto \rho^{-1/4}$.

We are interested in evaluating this near the mid-plane, where the characteristic magnetic field strength in the ISM, B_*, is given by

$$B_* = \frac{\sqrt{2\pi\rho_*}}{M_A}\sigma = \sqrt{\frac{2\ G}{f_{\rm gas}}}\frac{\pi\ \Sigma_{\rm gas}}{M_A} \tag{53}$$

Making this substitution, with a bit of algebra we obtain

$$K_* \simeq \frac{1}{3\beta}\left(\frac{E_{\rm CR} M_A}{e\sigma^2}\sqrt{\frac{G}{2 f_{\rm gas}}}\right)^p \simeq 0.25\ M_A^{1/2} E_{\rm CR,0}^{1/2} f_{\rm gas}^{-1/4} \sigma_1^2 \tag{54}$$

where $E_{\rm CR,\,0} = E_{\rm CR}/1$ GeV (and we have adopted the fiducial $p = 1/2$ for the numerical evaluation). However, note the general restriction that $K_* \geq 1$, since this is the limit set by convective transport of CRs; thus galaxies with low velocity dispersions will be in this convective limit.

As discussed by Zweibel (2017) among others, it is important to distinguish between the case where the turbulent Alfvén waves that scatter CRs is balanced, that is, roughly equal power in Alfvén waves propagating in both directions along a field line, and unbalanced, where the Alfvén waves are predominantly in a single direction. In the latter case, the CRs can stream with the Alfvén waves (although the transport is still dominated by scattering rather than streaming, i.e. streaming does little to increase the value of K_*), and streaming losses occur. In the former, streaming losses due to Alfvén waves propagating in one direction are compensated by energy gain from waves propagating in the opposite direction, and there is no net streaming loss; indeed, there may be a net gain of energy by the CRs due to second-order *Fermi* acceleration. For the present CR transport model, we are interested in a case where the majority of the stellar feedback driving the turbulence is injected near the mid-plane. Thus, we will assume that the Alfvén modes in the turbulence

[10]Note that Farber et al. (2018) present numerical MHD simulations where they try to incorporate the effect of ion-neutral damping on CR transport in neutral ISM gas via the expedient of a diffusion coefficient that *increases* by a factor of 10–3.0 × 10^{28} cm^2 s^{-1} in gas below a temperature of 10^4 K. However, we find that transport is not necessarily faster for the ‘Streaming’ case than for the ‘Scattering’ case; in general this depends on χ, $f_{\rm gas}$, and other properties, as can be seen by comparing equation (47) to the equivalent expression for scattering derived below, equation (57). Over the range of properties explored by observed galaxies, one can find regimes where both scattering and streaming give larger diffusion coefficients. We also find that, for the range of parameters we expect to encounter in galaxies, the ‘Streaming’ diffusion coefficient is substantially lower than Farber et al.’s assumed 3.0 × 10^{28} cm^2 s^{-1}.

are unbalanced, with waves leaving the mid-plane predominating. In this case, the effective speed that determines the streaming loss is $v_s = v_A$, and the streaming[11] and absorption optical depths are therefore

$$\tau_{\rm stream} = \frac{\beta}{\sqrt{2}M_A}\left(\frac{E_{\rm CR}M_A}{e\sigma^2}\sqrt{\frac{G}{2f_{\rm gas}}}\right)^{-p} \simeq 0.96\, M_A^{-3/2} E_{\rm CR,0}^{-1/2} f_{\rm gas}^{1/4}\sigma_1^2 \tag{55}$$

and

$$\tau_{\rm abs} = \tau_{\rm pp}\left(\frac{E_{\rm CR}\, M_A}{e\sigma^2}\sqrt{\frac{G}{2f_{\rm gas}}}\right)^{-p} \simeq 1.3\, M_A^{-1/2} E_{\rm CR,0}^{-1/2} f_{\rm gas}^{1/4}\sigma_1\Sigma_{\rm gas,1}. \tag{56}$$

Again, note that these expressions are valid for $K_* > 1$.

For this model, the dimensional diffusion coefficient and escape time, for $K_* > 1$, are

$$\kappa_* = 9.4\times 10^{25}\, M_A^{1/2} E_{\rm CR,0}^{1/2} f_{\rm gas}^{3/4}\frac{\sigma_1}{\Sigma_{\rm gas,1}}\ {\rm cm^2\ s^{-1}} \tag{57}$$

$$t_{\rm esc,diff} = 440\, M_A^{-1/2} E_{\rm CR,0}^{-1/2} f_{\rm gas}^{5/4}\frac{\sigma_1^3}{\Sigma_{\rm gas,1}}\ {\rm Myr}. \tag{58}$$

The corresponding values for $K_* = 1$ are given by equations (16) and (39), respectively. The streaming loss time is

$$t_{\rm stream} = \frac{3z_*}{v_A} = 150\frac{M_A f_{\rm gas}\sigma_1}{\Sigma_{\rm gas,1}}\ {\rm Myr}, \tag{59}$$

and the collisional loss time is independent of the CR transport model (equation 49). Thus, in this CR transport model streaming losses occur a factor of a few more slowly than collisional losses even for MW-like conditions, and become even less important in higher surface density galaxies.

2.3.3 *Constant diffusion coefficient*

Our final, purely empirical, model is simply to plead ignorance as to the true value of the diffusion coefficient as a function of galaxy properties, and adopt the empirically determined MW one for all galaxies: $\kappa_* \approx \kappa_{*,\rm MW} \equiv 1\times 10^{28}$ cm^2 s^{-1}, as estimated empirically for ~GeV CRs in the MW (e.g. Ptuskin et al. 2006). In our dimensionless variables, this corresponds to

$$K_* = \frac{\kappa_{*,\rm MW}}{\kappa_{\rm conv}} \simeq 2.6\frac{\Sigma_{\rm gas,1}}{f_{\rm gas}\sigma_1^3}. \tag{60}$$

Note that this assumption can produce $K_* < 1$, which is unphysical, but we do not enforce this condition for the purposes of comparing to previous works in which κ_* has been treated as constant. For this model, we also adopt $v_s = v_A$, in which case we have

$$\tau_{\rm stream} = \frac{1}{\sqrt{2}M_A K_*} = 0.27\frac{f_{\rm gas}\sigma_1^3}{M_A\Sigma_{\rm gas,1}} \tag{61}$$

$$\tau_{\rm abs} = \frac{\tau_{\rm pp}}{K_*\beta} = 0.37 f_{\rm gas}\sigma_1^2. \tag{62}$$

[11]Note that, for this scattering case – and for the case of constant diffusion coefficient outlined below – the optical depth to *scattering* is given by $z_*/\lambda_{\rm mfp} = cz_*/(3\kappa_*) = 1/\beta_A\tau_{\rm stream}$. Thus, while we shall find below that $\tau_{\rm stream} \lesssim 1$ for parameters apposite to real galaxies and for the 'scattering' and constant κ_* cases, at the same time, we find scattering optical depths $\gtrsim$ 1000 and $\gtrsim$ 100 for these two cases, respectively so we are, again, well into the diffusive regime. The CR optical depth to scattering is the direct analogue to what Socrates et al. (2008) label $\tau_{\rm CR}$.

Table 3. Example galaxy parameters. The range given for $\Sigma_{\rm gas}$ is the approximate range in galaxy surface densities over which the indicated parameter sets are plausible.

Quantity	Galaxy model		
	Local	Intermediate	Starburst
$\Sigma_{\rm gas}$ (M$_\odot$ pc^{-2})	10^0–$10^{2.5}$	10^1–$10^{3.5}$	$10^{2.5}$–$10^{4.5}$
σ (km s^{-1})	10	30	100
$f_{\rm gas}$	0.1	0.4	0.7
χ	10^{-2}	10^{-3}	10^{-4}

The diffusive escape time is

$$t_{\rm esc,diff} = 21 f_{\rm gas}^2\frac{\sigma_1^4}{\Sigma_{\rm gas,1}^2}\ {\rm Myr}, \tag{63}$$

and the streaming time-scale is identical to that in the scattering model (equation 59).

2.3.4 *Comparison of transport models*

Before proceeding to apply the various CR transport models, it is helpful to develop some intuition by comparing their predictions for the key dimensionless (K_*, $\tau_{\rm abs}$, $\tau_{\rm stream}$) and dimensional (κ_*, $t_{\rm esc,\,diff}$, $t_{\rm col}$, $t_{\rm stream}$) parameters that describe the system as a function of galaxy gas surface density. Since these quantities also depend on additional quantities such as the gas velocity dispersion and gas fraction, it is helpful to consider a few cases that are representative of different types of galaxies. We consider three parameter sets, which we can imagine as describing typical values in local spiral galaxies, starburst/merger systems, and a case intermediate between these extremes. We summarize the parameters, we adopt for these three cases in Table 3. In all cases, we adopt $M_A = 1.5$ and $E_{\rm CR} = 1$ GeV.

We plot dimensionless and dimensional parameters for our CR transport models in Fig. 1. The figure allows a few immediate observations. First focus on the top two rows, showing K_* and κ_*. The streaming and scattering models give nearly identical values of K_* and κ_* for local galaxy conditions. However, the two models change in different directions as we shift from the local to the starburst regime: a scattering model predicts less and less efficient diffusion in higher surface density galaxies, eventually saturating at the convection limit, while the streaming model predicts more rapid transport in starburst galaxies due to the higher neutral fraction, and thus higher streaming speed, in these galaxies interstellar media. The constant κ_* model is qualitatively different. For the other models, as the gas surface density rises, reducing the scale height and increasing the density, the CR diffusion coefficient goes down. If one assumes constant κ_*, this does not happen, and K_* can be far larger or smaller than the convective value. The former is certainly unphysical, and the latter is likely unrealistic as well, and thus we will not consider the constant κ_* model further in this work.

Now consider the lower two rows, which show the dimensionless scattering and absorption optical depths, and the loss times. Again, we can make a few immediate observations. At higher gas surface densities, $\tau_{\rm abs}$ always becomes larger than unity, and $t_{\rm col}$ smaller than $t_{\rm esc,\,diff}$ or $t_{\rm stream}$. Thus we expect galaxies to become increasingly calorimetric and dominated by collisional losses as we go from low to high gas surface density, with a transition to calorimetry occurring at ~100–1000 M$_\odot$ pc^{-2} depending on model parameters. The sole exception to this is if one assumes constant κ_*, in which case the ratio of escape to collisional loss time is independent of gas surface

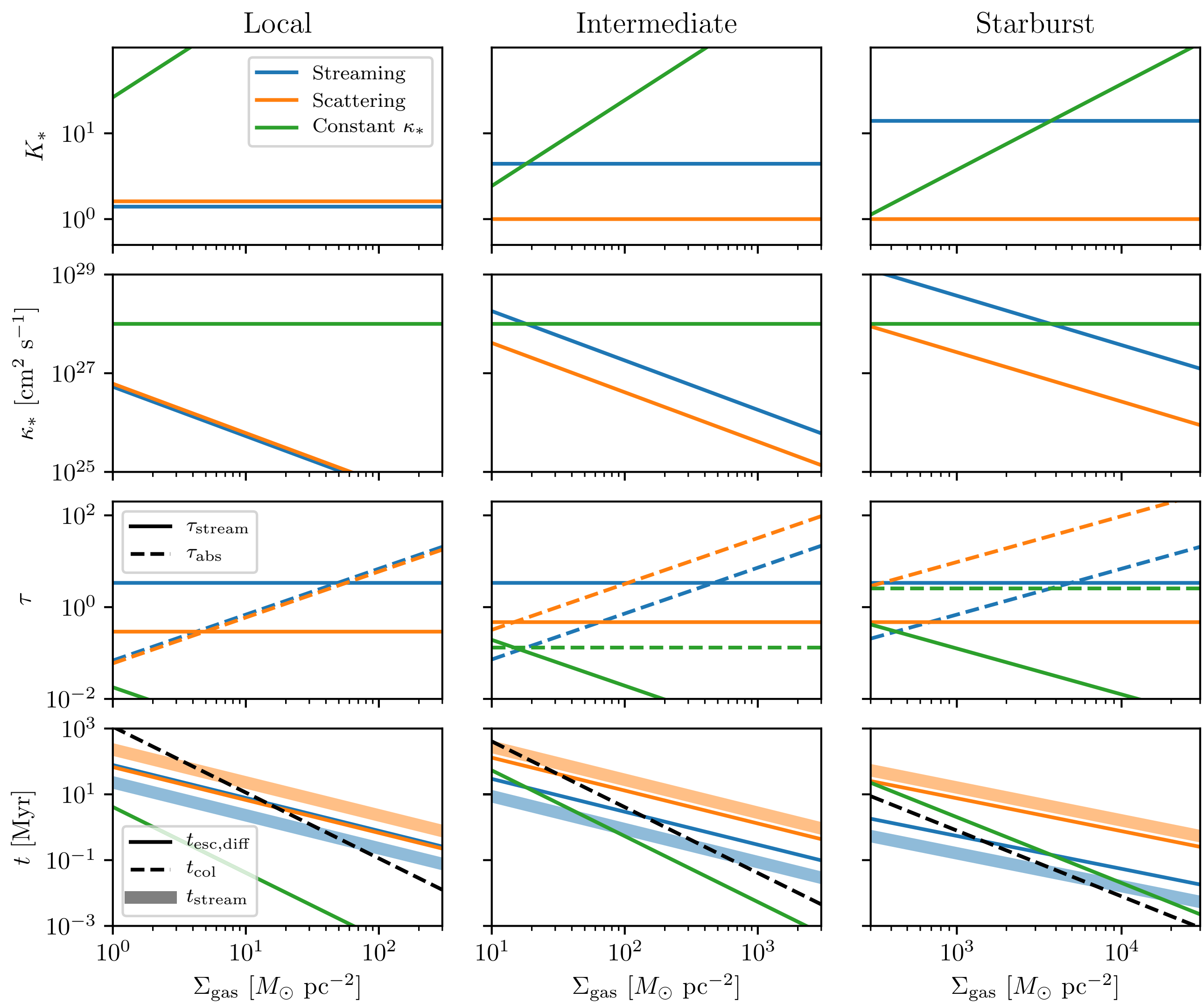

Figure 1. Dimensionless (K_*, $\tau_{\rm stream}$, $\tau_{\rm abs}$) and dimensional (κ_*, $t_{\rm esc,\,diff}$, $t_{\rm col}$, $t_{\rm stream}$) quantities as a function of gas surface density predicted by our CR transport models. The three columns are for the local, intermediate, and starburst cases, whose parameters are given in Table 3. Note that the horizontal axis range is different for each column; we have limited to axis range to gas surface densities that are reasonably plausible for each particular set of parameters.

density; again, this is unphysical. A second result of note is the relative size of the streaming optical depth $\tau_{\rm stream}$ and streaming loss time $t_{\rm stream}$ in the different models. Streaming losses are strongest in the streaming case, and thus should play a significant role over nearly all of parameter space. They are comparably much less important for a scattering transport model.

3 COSMIC RAY EQUILIBRIA

Having obtained our dimensionless equations and considered the microphysics of CR transport, we now proceed to explore the properties of CR equilibria.

3.1 Numerical method

While it is possible to solve equations (30) and (33) analytically in certain limiting cases, in general they must be solved numerically. Our first step is therefore to develop an algorithm to obtain solutions. Because the boundary conditions, equations (35)–(38), are specified at different points (two at $\xi = 0$ and two at $\xi = \infty$), the system is a boundary value problem, which we must solve iteratively.

Our first step is to make a change of variables to a form that renders the system somewhat more stable for numerical integration. We use as our integration variables s, $\ln(\mathrm{d}s/\mathrm{d}\xi) \equiv \ln r$, $\ln p_c$, and $f_c \equiv \mathcal{F}_c/K_*\beta p_c$; intuitively, these quantities are the column density, the logarithmic volume density, the logarithmic CR pressure, and the effective CR propagation speed. In terms of these variables, equations (30) and (33), and their boundary conditions (equations 35–38) become

$$\frac{\mathrm{d}}{\mathrm{d}\xi}\begin{pmatrix} s \\ \ln r \\ \ln p_c \\ f_c \end{pmatrix} = \begin{pmatrix} r \\ \phi_{\rm B}^{-1}\left(f_{\rm gas} - 1 - f_{\rm gas} s + p_c r^{q-1} f_c\right) \\ -r^q f_c \\ -\tau_{\rm abs} r - \tau_{\rm stream} r^q f_c + r^q f_c^2 \end{pmatrix}, \qquad (64)$$

with boundary conditions $s(0) = 0$, $\lim_{\xi\to\infty} s(\xi) = 1$, $f_c(0) = f_{\rm Edd}/p_c(0)$, and $\lim_{\xi\to\infty} f_c(\xi) = 4\tau_{\rm stream,\,\infty}$.

We then solve this system using a shooting algorithm: we have $s(0) = 0$ from equation (35), and we start with an initial guess for the mid-plane log density $\ln r(0)$ and CR pressure $\ln p_c(0)$.

These choices together with equation (36) allow us to compute the effective propagation speed $f_c(0)$ at the mid-plane, so that we now have a set of four initial values at $\xi = 0$. We can then integrate the system outward toward $\xi \to \infty$, stopping when either (1) s and f_c both approach constant values, or (2) $\ln r$ or $\ln p_c$ diverge to negative infinity, or (3) f_c diverges to positive infinity. The integration must be carried out with care, since at large ξ the system becomes extremely sensitive to numerical noise; we use a fourth-order implicit Runge–Kutta method to maintain stability. We then carry out a double-iteration procedure: we hold $\ln r(0)$ fixed and iteratively adjust $\ln p_c(0)$ until we find a value such that $\lim_{\xi \to \infty} f_c = 4\tau_{\rm stream}$ (equation 38). This choice will not in general satisfy the condition that $\lim_{\xi \to \infty} s(\xi) = 1$ (equation 35), and thus we next iteratively adjust $\ln r(0)$ until this boundary condition is satisfied. We note that, for sufficiently large $f_{\rm Edd}$, the procedure does not converge, and it is not possible to find a solution that satisfies the boundary conditions. We defer further discussion of this case to the companion paper, CKT20b.

3.2 Gas density and cosmic ray pressure profiles

Our next step, now that we have an algorithm to generate solutions, is to develop some intuition for the behaviour of solutions and their dependence on the four fundamental parameters for our system: $\tau_{\rm stream}$ (equation 31), $\tau_{\rm abs}$ (equation 32), $f_{\rm Edd}$ (equation 36), and $f_{\rm gas}$. We plot example dimensionless gas density and CR pressure profiles in Fig. 2. In each of the four panels shown, we vary one quantity, as indicated in the legend, while holding the other three constant; the quantities not indicated in the legend have values $\log f_{\rm Edd} = 10^{-0.75}$, $\tau_{\rm abs} = 1$, $\tau_{\rm stream} = 1$, and $f_{\rm gas} = 0.5$, and in all cases we adopt our fiducial values $\phi_{\rm B} = 1.01$ and $q = 1/4$. The range of parameters we have chosen are representative of the range found in observed galaxies, as we discuss below.

We can understand the results shown in each of the panels intuitively. In the top panel, we see that smaller values of $f_{\rm Edd}$ yield (not surprisingly) smaller CR pressures, and density profiles that are close to the values that would be obtained absent CR pressure. As $f_{\rm Edd}$ rises, the density profile becomes more extended and develops a long tail at high ξ that is supported by CR pressure (cf. Ghosh & Ptuskin 1983; Chevalier & Fransson 1984; Ko et al. 1991). At the highest $f_{\rm Edd}$, a mild density inversion appears near $\xi = 0$. We show in Appendix B that in such regions the solution becomes Parker unstable, but that this is unlikely to significantly modify any of our conclusions. We therefore ignore Parker stability considerations for the remainder of the main text.

Turning to the second and third panels, we see that $\tau_{\rm abs}$ and $\tau_{\rm stream}$ mainly control how rapidly the CR pressure drops with ξ – larger opacities lead to sharper drops, as more and more CRs are lost to absorption or streaming. The value of $\tau_{\rm stream}$ has more dramatic effects than the value of $\tau_{\rm abs}$, because $\tau_{\rm stream}$ not only controls streaming losses, it controls the boundary condition at infinity: smaller $\tau_{\rm stream}$ corresponds to a smaller ratio of $F_c/(u_c + P_c)$ (i.e. less flux per unit CR enthalpy) as $z \to \infty$. Thus, smaller τ_s implies larger CR pressure and energy at large z.

Finally, we see that the gas fraction has relatively small effects on either the density or CR pressure profiles. More gas-rich systems experience more flattening of the density profile near $\xi = 0$ as a result of CR pressure support; this is simply a consequence of the fact that the gravitational acceleration builds up more slowly with ξ for larger $f_{\rm gas}$, and thus gravity is weaker near the mid-plane, making it easier for CR pressure to flatten the density profile.

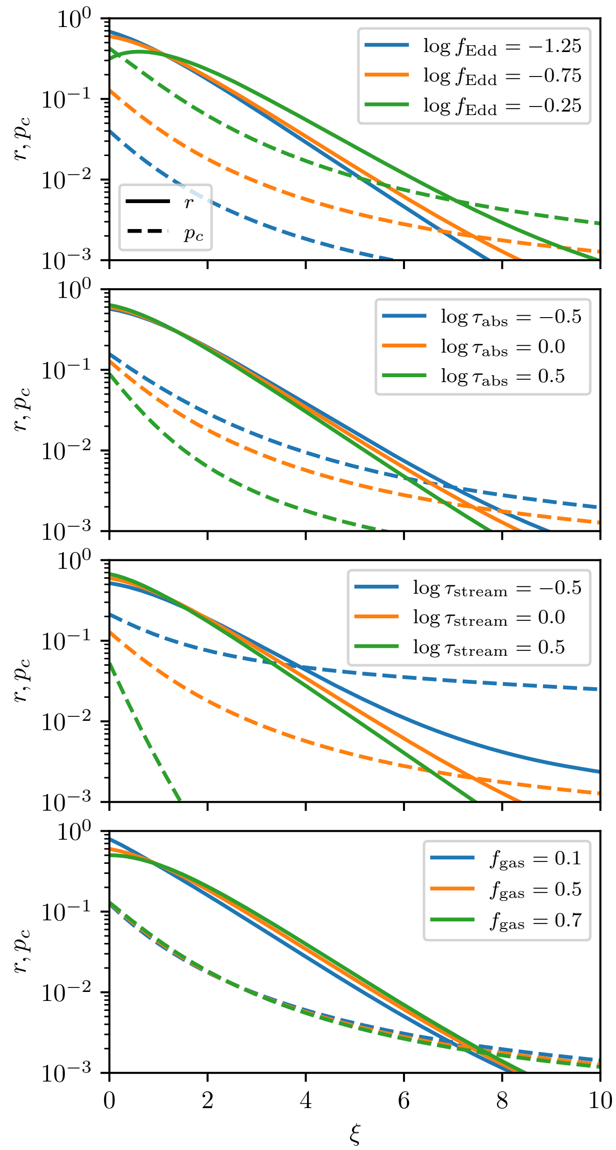

Figure 2. Profiles of (dimensionless) volumetric density $r(\xi)$ (solid) and (dimensionless) CR pressure $p_c(\xi)$ (dashed). In each panel, one of the four fundamental parameters – $f_{\rm Edd}$, $\tau_{\rm abs}$, $\tau_{\rm stream}$, and $f_{\rm gas}$ – is varied (as indicated in the legend), while the other three are held constant; the constant values we adopt are $f_{\rm Edd} = 10^{-0.25}$, $\tau_{\rm abs} = 1$, $\tau_{\rm stream} = 1$, and $f_{\rm gas} = 0.5$.

3.3 Cosmic ray pressure contribution and calorimetry

In this paper, we are interested in where CRs are dynamically important for helping support the ISM, and we are now in a position to answer this question in the context of our models. Fig. 3 shows the ratio of CR to turbulent pressure computed for a sample of parameters. We show this ratio computed in two ways: the mid-plane value (dashed lines), and the average value of the first gas scale height (solid lines). For this purpose, we define a scale height to be the value of ξ for which $s(\xi) = 1 - e^{-1}$, that is, the scale height is defined as the height for which the fraction of the gas mass below that height has the same value as it would at one scale height in an exponential atmosphere. Clearly we see that, as $f_{\rm Edd}$ is dialled upwards, the CRs make a larger and larger contribution to the total pressure, becoming dominant at sufficiently large $f_{\rm Edd}$; indeed, for sufficiently large $f_{\rm Edd}$, the mid-plane density drops to zero (as indicated by the dashed lines

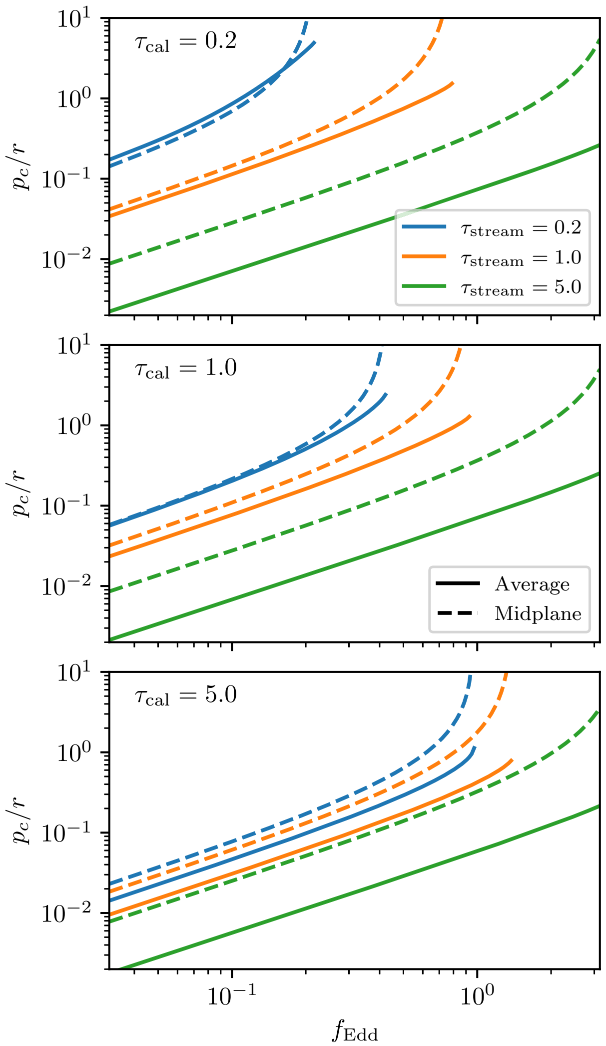

Figure 3. Ratio of CR pressure to gas turbulent pressure $p_c/r = P_c/P_{\rm gas}$ as a function of $f_{\rm Edd}$, for absorption optical depths $\tau_{\rm abs} = 0.2$, 1.0, and 5.0 (top to bottom panels), and for $\tau_{\rm stream} = 0.2$, 1.0, and 5.0 (colours, as indicated in the legend). All cases shown use $f_{\rm gas} = 0.5$, but results are qualitatively similar for any $f_{\rm gas}$. In each case, dashed lines show the ratio measured at the mid-plane, while solid lines show the ratio averaged over the first gas scale height.

in the figure diverging to infinity), and no hydrostatic equilibrium is possible, a topic to which we return in Paper II. We truncate the lines in the plot when this condition occurs. We also see that the CR pressure contribution drops as we increase the optical depth due to the increasing importance of losses, particularly as one moves away from the mid-plane. For the highest optical depth cases shown in Fig. 3, the ratio of CR pressure to gas pressure is almost an order of magnitude smaller averaged over the scale height than at the mid-plane, due to the rapid loss of CRs with height when $\tau_{\rm abs}$ or $\tau_{\rm stream}$ are large. Conversely, at low optical depth and low $f_{\rm Edd}$, the ratio of CR pressure to gas pressure averaged over a scale height is generally *larger* than it is at the mid-plane, due to the larger scale height of the CRs compared to the gas in these models.

The primary observational signature of hadronic CRs beyond the MW is γ-ray emission, and it is therefore interesting to ask what fraction of relativistic CRs are absorbed in collisions (i.e. lost to pion production) and thus are available to produce observable γ-rays. We

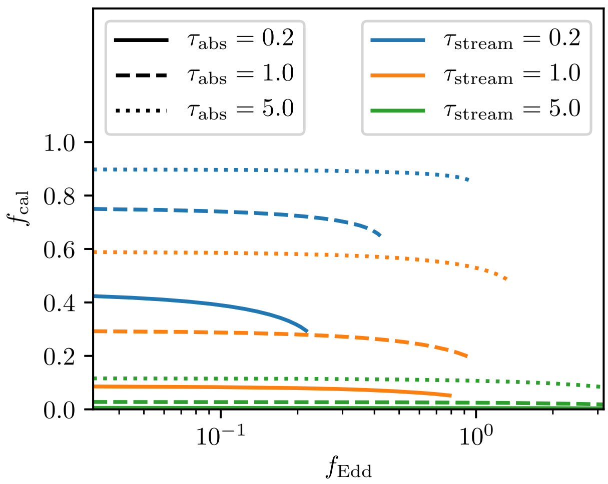

Figure 4. Fraction of CRs flux $f_{\rm cal}$ lost to *pp* collisions, and thus available to produce γ-ray emission, as a function of $f_{\rm Edd}$. We show solutions for a sample of absorption and streaming optical depths $\tau_{\rm abs}$ (solid, dashed, and dotted lines) and $\tau_{\rm stream}$ (blue, orange, and green lines), as indicated in the legend. The cases shown are the same as in Fig. 3.

can compute this calorimetric fraction from our solutions for the density and pressure profiles $r(\xi)$ and $p_c(\xi)$ in two ways. One is simply to note that the rate per unit volume at which CRs are lost to *pp* collisions is $u_c/t_{\rm col}$. Thus, if we integrate over the full gas column, and then divide by the flux $F_c(0)$ of CRs injected per unit area, we have

$$f_{\rm cal} = \frac{1}{F_c(0)} \int_0^\infty \frac{u_c}{t_{\rm col}}. \tag{65}$$

It is straightforward, if algebraically tedious, to rewrite the RHS in terms of non-dimensional quantities using the transformations given in Section 2.2. However, one can obtain the same result with significantly more insight by instead starting from the dimensionless CR transport equation, equation (30). Let us define $q = -(\mathrm{d}s/\mathrm{d}\xi)^{-q}\mathrm{d}p_c/\mathrm{d}\xi = \mathcal{F}_c/K_*\beta$ as the dimensionless, scaled CR flux; from equation (36), we have $q(0) = f_{\rm Edd}$. If we now divide both sides of equation (30) by the injected CR flux $q(0)$ and then integrate from 0 to ξ, the result is

$$\frac{q(\xi)}{f_{\rm Edd}} = 1 - \frac{\tau_{\rm abs}}{f_{\rm Edd}} \int_0^\xi r p_c \,\mathrm{d}\xi - \frac{\tau_{\rm stream}}{f_{\rm Edd}} \left[p_c(0) - p_c(\xi)\right]. \tag{66}$$

This expression has a simple physical interpretation: the quantity on the LHS, $q(\xi)/f_{\rm Edd}$, is simply the fraction of the flux that was injected at $\xi = 0$ that remains once the CRs have gotten to height ξ. The RHS asserts that this fraction is equal to unity minus the flux that has been lost to absorption/pion losses (the term proportional to $\tau_{\rm abs}$) and to streaming losses (the term proportional to $\tau_{\rm stream}$). We can therefore identify the fraction of the flux that goes into pion production as

$$f_{\rm cal} = \frac{\tau_{\rm abs}}{f_{\rm Edd}} \int_0^\infty r p_c \,\mathrm{d}\xi. \tag{67}$$

In Fig. 4, we show calculations of $f_{\rm cal}$ for the same set of models as shown in Fig. 3. Clearly, the value of $f_{\rm Edd}$ has relatively little effect on $f_{\rm cal}$. Instead, the dominant parameters controlling $f_{\rm cal}$ are the streaming and absorption optical depths. If $\tau_{\rm abs} > \tau_{\rm stream}$ and $\tau_{\rm abs} > 1$, then a majority of the CRs are absorbed and can produce γ-ray emission. By contrast, if $\tau_{\rm stream} \gtrsim \tau_{\rm abs}$ or $\tau_{\rm abs} < 1$, then $f_{\rm cal}$ is much smaller.

3.4 Model grid

Having developed some intuition for how the results of interest depend on the model parameters, we now generate a broad grid of solutions and extract pertinent parameters from them. Our grid consists of gas fractions $f_{\rm gas}$ from 0 to 1 in steps of 0.1, log Eddington ratios $\log f_{\rm Edd}$ from 10^{-4} to 10 in steps of 0.025 dex, log absorption optical depths $\log \tau_{\rm abs}$ of $10^{-1.5}$–10^{2} in steps of 0.25 dex, and log streaming optical depths $\log \tau_{\rm stream}$ of 10^{-1}–10^{1} in steps of 0.25 dex. Note that, for large enough $f_{\rm Edd}$, the model does not converge, and no equilibrium exists; we defer further discussion of this behaviour to Paper II. For each grid point where a solution is found, we record the mid-plane density and pressure, $r(0)$ and $p_c(0)$ and the fraction $f_{\rm cal}$ of the CR flux that is absorbed and therefore available for pion production (equation 67).

4 IMPLICATIONS FOR STAR-FORMING SYSTEMS

4.1 Dimensionless parameters for observed systems

We now have in hand machinery required to calculate the quantities of interest for any combination of dimensionless parameters. For a specified choice of CR propagation model, we also have in hand the mapping from galaxy gas surface density $\Sigma_{\rm gas}$, velocity dispersion σ, and gas fraction $f_{\rm gas}$, to the dimensionless optical depths $\tau_{\rm stream}$ and $\tau_{\rm abs}$ (Table 2). The final dimensionless quantity we require is the Eddington ratio $f_{\rm Edd}$ (equation 36). This depends on the reference flux F_* (equation 22) and on the injected CR flux $F_{c,0}$. We choose to write the latter in terms of the SFR, as

$$F_{c,0} = \epsilon_{c,1/2}\dot{\Sigma}_\star, \tag{68}$$

where $\epsilon_{\rm c,\,1/2}$ is the mean total energy in relativistic CRs released into each galactic hemisphere per unit mass of star formation. This yields

$$\begin{aligned} f_{\rm Edd} &= \epsilon_{c,1/2}\left(\frac{\tau_{\rm stream}}{\beta_s}\right)\frac{f_{\rm gas}\dot{\Sigma}_\star}{\pi G c \Sigma_{\rm gas}^2} \\ &= 2.0 f_g K_* \dot{\Sigma}_{\star,-3}\sigma_1^{-1}\Sigma_{\rm gas,1}^{-2}, \end{aligned} \tag{69}$$

where $\dot{\Sigma}_{\star,-3} = \dot{\Sigma}_\star/10^{-3}$ M$_\odot$ pc^{-2} Myr^{-1}, and the numerical evaluation is for our fiducial value of the CR energy release per unit mass of stars formed, $\epsilon_{c,\,1/2} = \epsilon_{c,\,*,\,1/2}$ (see below). This equation contains a crucial result, which will become important later in our discussion: constant Eddington ratio corresponds roughly to $\dot{\Sigma}_\star \propto \Sigma_{\rm gas}^2$.

Accounting only for CR acceleration associated with core-collapse SNe, a reference value for the CR energy release per unit mass of star formation into each Galactic hemisphere, $\epsilon_{\rm c,\,1/2}$, can be defined as

$$\begin{aligned} \epsilon_{\rm c,1/2} &\simeq \frac{1}{2}\frac{\eta_{\rm c}\,E_{\rm SN}}{M_{\star,\rm SN}} \\ &\equiv \epsilon_{\rm c,\star,1/2}\left(\frac{\eta_{\rm c}}{0.1}\right)\left(\frac{E_{\rm SN}}{10^{51}\,\rm erg}\right)\left(\frac{90\,\rm M_\odot}{M_{\star,\rm SN}}\right) \end{aligned} \tag{70}$$

where $\eta_{\rm c} \sim 0.1$ is a rough (e.g. Drury, Markiewicz & Voelk 1989; Hillas 2005; Strong et al. 2010; Lacki et al. 2010; Paglione & Abrahams 2012; Peng et al. 2016) calibration for the fraction of the total core collapse SN kinetic energy release that ends up in CRs, $E_{\rm SN}$ is the SN kinetic energy, and, for a Chabrier (2005) IMF (initial mass function), one core-collapse SN requires the formation of $M_{\star,\,\rm SN} \simeq 90\,\rm M_\odot$ of stars assuming that all stars born with masses of 8 M$_\odot$ or above end their lives as core-collapse SNe. Numerically, the normalizing CR efficiency is

$$\epsilon_{\rm c,\star,1/2} \equiv 5.6\times10^{47}\ {\rm erg\ M_\odot^{-1}}\,. \tag{71}$$

Note that this normalization for $\epsilon_{\rm c,\,1/2}$ may be too conservative as it ignores other sources of mechanical power that may end up in CRs including stellar wind shocks, pulsar winds, and thermonuclear SNe. It also neglects the possibility, for which there is some evidence (Nomoto et al. 2006), that the mean mechanical energy per core-collapse SN might exceed by a factor of a few the canonical 10^{51} erg, and that a fraction of massive star core collapses end in black hole formation with potentially much weaker SNe, or none at all (e.g. Pejcha & Thompson 2015; Gerke, Kochanek & Stanek 2015). Finally, this normalization neglects the possibility that some fraction of CRs produced may be trapped in the SN-driven hot phase of the ISM and then advected out of the galaxy in a galactic wind while having relatively little interaction with the neutral phase; CRs that follow this path contribute to neither pressure support nor γ-ray emission, and thus advective escape of hot gas might lower the effective value of $\epsilon_{c,\,1/2}$. (Advective escape of neutral gas is likely unimportant, since, even in the galaxies with the strongest winds, only a small fraction of the neutral material is ejected per dynamical time.) We will ignore these complications in the remainder of this paper, however.

We show values of $f_{\rm Edd}$ and $\tau_{\rm abs}$ for a sample of galaxies culled from the literature in Fig. 5, computed adopting the 'Streaming' model for CR transport (Section 2.3.1) with $M_A = 1.5$; we do not show $\tau_{\rm stream}$, since for the 'Streaming' model it is simply M_A^3, and thus is constant for all galaxies. We compare to the 'Scattering' model, and explore the dependence on M_A, in Section 4.4. The data come from the compilation of Krumholz et al. (2012), and consist of measurements of gas surface density $\Sigma_{\rm gas}$ and SFR surface density $\dot{\Sigma}_\star$. We also add a point to represent conditions in the Solar neighbourhood, which has $\Sigma_{\rm gas} \approx 14$ M$_\odot$ pc^{-2} (McKee, Parravano & Hollenbach 2015) and $\dot{\Sigma}_\star \approx 2.5\times10^{-3}$ M$_\odot$ pc^{-2} Myr^{-1} (Fuchs, Jahreiß & Flynn 2009). Since velocity dispersions and gas fractions are only available in the literature for a small subset of these galaxies, we assign values as follows: for the sample of Kennicutt (1998), we adopt 'Local' parameters for all galaxies classified as spirals by Kennicutt, and we also adopt these properties for the Solar neighbourhood; for those classified as starburst, we adopt 'Intermediate' parameters if the gas surface density is below 10^3 M$_\odot$ pc^{-2}, and 'Starburst' parameters otherwise. We adopt 'Intermediate' parameters for the entire sample of galaxies from Daddi et al. (2008, 2010a) and Tacconi et al. (2013), and for all galaxies from the sample of Genzel et al. (2010) except those that Genzel et al. classify as sub-mm galaxies, for which we use 'Starburst' parameters. Finally, we also apply 'Starburst' parameters for the sample of sub-mm galaxies taken from Bouché et al. (2007). We illustrate the classifications in Fig. 6; for reference, we also overlay on this figure the Kennicutt (1998) fit for the relationship between star formation and gas surface densities.[12] Similarly, in order to overlay rough contours on Fig. 5, we linearly interpolate $\log\sigma$, $\log f_{\rm gas}$, and $\log\chi$ as a function of $\log\Sigma_{\rm gas}$ between the three cases listed in Table 3, treating each case as a single point at the centre of the

[12]Note that the Kennicutt (1998) line shown in Fig. 6 does not in fact pass through the data points in the Kennicutt (1998) sample. This is because the data points have been adjusted to use updated estimates of the conversion from CO luminosity to gas surface density, and from IR or Hα luminosity to star formation surface density, following Daddi et al. (2010a). However, we choose not to adjust the fit for these updates, in part to maintain consistency with earlier work, and in part because the fit remains a reasonable one for the expanded data set shown in the figure.

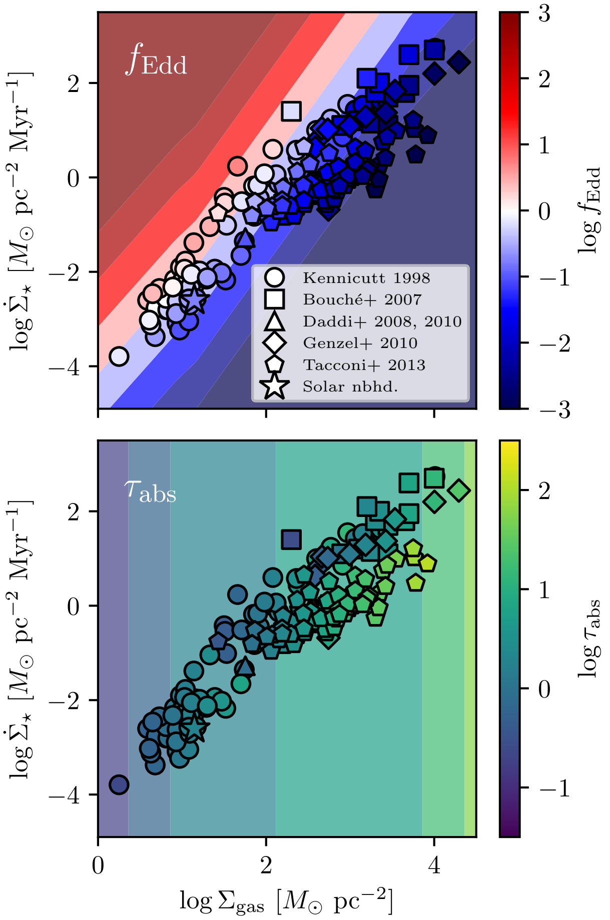

Figure 5. Distribution of $f_{\rm Edd}$ (top panel) and $\tau_{\rm abs}$ (bottom panel) values for a sample of observed galaxies culled from the literature, computed using the 'Streaming' CR transport model. Points are coloured by the value of $f_{\rm Edd}$ or $\tau_{\rm abs}$ that we infer for that galaxy, following the discussion in the main text; colour bars indicate numerical values, and the shape of the symbol indicates the sample from which it is drawn: Kennicutt (1998), Bouché et al. (2007), Daddi et al. (2008, 2010a), Genzel et al. (2010), or Tacconi et al. (2013); the star indicates Solar neighbourhood conditions, for which we adopt values described in the main text. Coloured contours indicate regions of the plane with values of $\log f_{\rm Edd}$ from -3 to 3 in steps of 1 and $\log \tau_{\rm abs}$ from -1.5 to 2.5 in steps of 0.5, respectively, for the streaming CR propagation model Section 2.3.1, using gas fractions, velocity dispersions, and ionization fractions interpolated as a function of $\Sigma_{\rm gas}$ as described in the main text.

stated range. However, we emphasize that all these classifications and parameter choices are approximate. More accurate estimates would use values of the gas fraction and velocity dispersion determined galaxy-by-galaxy, and estimates of χ based on detailed chemical modelling (cf. Krumholz et al. 2020).

The primary conclusion to be drawn from the figure is that, as one proceeds along the star-forming galaxy sequence from low to high gas and star formation surface density, galaxies become increasingly sub-Eddington and optically thick to CRs. Local spirals and dwarfs tend to have $f_{\rm Edd} \sim 0.1$–1 and $\tau_{\rm abs} \ll 1$, while high-redshift galaxies and starbursts typically have $f_{\rm Edd} \sim 0.001$–0.1 and $\tau_{\rm abs} \sim 1$–10.

4.2 CR pressures

We show estimates for the mid-plane CR pressure, and the ratio of CR pressure to gas pressure, in Fig. 7; results for the average pressure

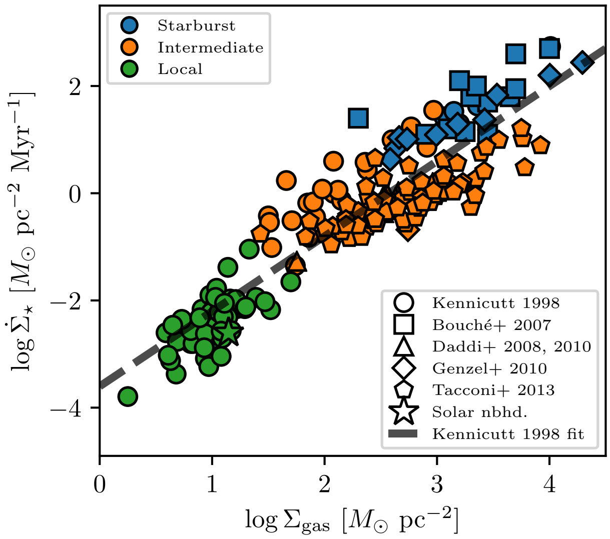

Figure 6. Illustration of our classification of galaxies in the Kennicutt–Schmidt plane as 'local', 'intermediate', and 'starburst'. Colour indicates the classification, while symbol shape indicates the sample from which the galaxy is drawn. Points match those shown in Fig. 5. For reference, we also overlay (dashed black line) the Kennicutt (1998) fit for the relationship between star formation and gas surface density.

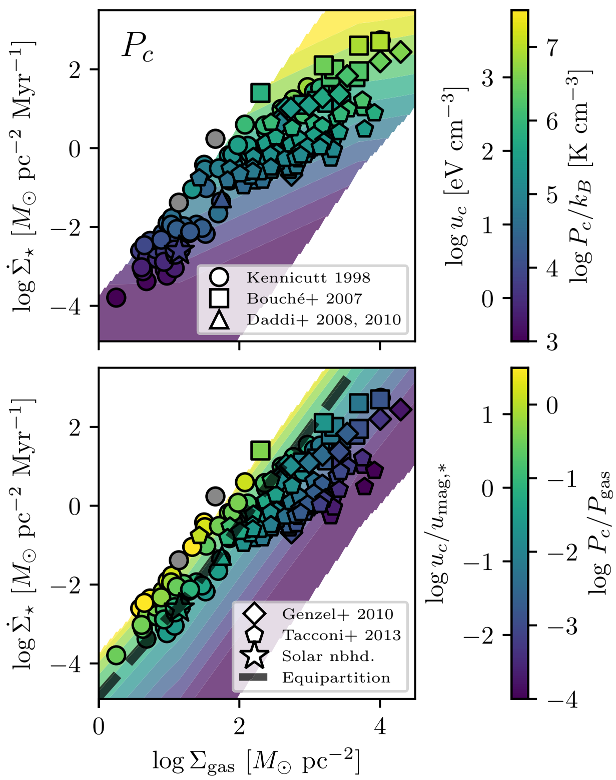

Figure 7. Estimated CR pressure and energy density (top panel) and ratio of CR pressure to gas pressure (bottom panel) at the galactic mid-plane for the sample of observed galaxies shown in Fig. 5 (coloured points), computed using the 'Streaming' CR transport model. Grey points mark galaxies whose Eddington ratios place them outside our grid. We also show contours of P_c and $P_c/P_{\rm gas}$, computed by interpolating as in Fig. 5. The contours of P_c run from $P_c/k_B = 10^3 - 10^{7.5}$ K cm^{-3} in steps of 0.5 dex, and the contours of $P_c/P_{\rm gas}$ run from 10^{-4}–$10^{0.5}$ in steps of 0.5 dex. Points that are not covered by contours correspond to combinations of parameters f_g, $f_{\rm Edd}$, $\tau_{\rm abs}$, and $\tau_{\rm stream}$ that are outside our grid of solutions. The black dashed line corresponds to the locus of equality between CR and magnetic energy densities.

over the first scale height are qualitatively similar. In order to generate these plots, for each galaxy we compute $\log f_{\rm Edd}$, $\log \tau_{\rm abs}$, $\log \tau_{\rm stream}$, and $f_{\rm gas}$ as described in Section 4.1, and then linearly interpolate on our grid of solutions (Section 3.4) to produce predicted values of $\log p_c$ and $\log r = \log({\rm d}s/{\rm d}\xi)$.[13] We then scale these back from dimensionless to physical units using the transformations given in Section 2.2. Similarly, we generate the contours in the background using the same interpolation scheme as described in Section 4.1.

We see that typical mid-plane CR pressures range from $P_c/k_B \sim 10^{3.5}$ K cm^{-3} (energy density $u_c \sim 1$ eV cm^{-3}) for sub-MW galaxies up to $\sim 10^7$ K cm^{-3} (energy density $\sim$few keV cm^{-3}) for the most intensely star-forming galaxies. Not surprisingly, mid-plane CR pressure increases with SFR. However, we also see that the ratio of CR pressure to gas pressure decreases systematically with SFR, such that $P_c/P_{\rm gas}$ is typically $\sim$0.1–1 for galaxies with $\Sigma_{\rm gas} \lesssim 100$ M$_\odot$ pc^{-2}, but drops to $\sim 10^{-3}$ for galaxies with $\Sigma_{\rm gas} \gtrsim 1000$ M$_\odot$ pc^{-2}. Contours of constant $P_c/P_{\rm gas}$ are close to lines of slope 2 in the lower panel of Fig. 7 (i.e. $\dot{\Sigma}_\star \propto \Sigma_{\rm gas}^2$), whereas the observed distribution of galaxies forms a significantly shallower relationship. Thus, we find that CRs are dynamically significant for weakly star-forming, low surface density galaxies, but become increasingly unimportant as we move to higher surface density, more strongly star-forming galaxies.

It is worth pointing out that, although we are comparing CR pressure to gas pressure in Fig. 7, we can also read the figure as describing the ratio of CR and magnetic energy densities, and thus the extent to which equipartition between CRs and magnetic fields holds. Defining the mid-plane magnetic energy density $u_{{\rm mag},*} = B_*^2/8\pi$, and making use of equation (53), we can write the ratio of CR to magnetic energy density at the mid-plane as

$$\frac{u_c}{u_{{\rm mag},*}} = 6M_A^2 \frac{P_c}{P_{\rm gas}}. \qquad (72)$$

Thus, for our fiducial choice $M_A = 1.5$, equipartition between CRs and magnetic fields corresponds to $P_c/P_{\rm gas} \simeq 0.1$. Thus, Fig. 7 can be read as also giving $u_c/u_{{\rm mag},*}$, if we simply shift the colour scale up by $\simeq 1$ dex, that is, $\log(P_c/P_{\rm gas}) \simeq -1$ corresponds to $u_c/u_{{\rm mag},*} \simeq 1$. We show the locus $u_c/u_{{\rm mag},*} = 1$ as the black dashed line in the lower panel of Fig. 7. We see that the Solar neighbourhood, and galaxies with similar conditions, are expected to show near-equipartition between CRs and magnetic fields. However, as we move to galaxies that are forming stars within increasing vigour, to the right of Fig. 7, CRs fall below equipartition with the magnetic field by 1–2 orders of magnitude (Thompson et al. 2006; Lacki et al. 2010; Lacki & Beck 2013).

It is worth noting that our conclusion that CR pressure is smaller than gas pressure in starbursts, and that the CR energy density is subequipartition, is consistent with the one-zone models developed by Lacki et al. (2010) to study the far-IR–radio correlation. We illustrate this in the top two panels of Fig. 8, where we show our estimated CR pressure and ratio of CR to gas pressure computed along the Kennicutt (1998) relation. That is, the figure is a parametric plot showing the values indicated by the contours in Fig. 7, calculated along a path through the $\Sigma_{\rm gas} - \dot{\Sigma}_\star$ plane given by the Kennicutt fit,

[13] A few galaxies, indicated by the grey points in Fig. 7, fall outside our grid, at values of $f_{\rm Edd}$ too high for a solution to exist. We discuss the significance of the maximum value of $f_{\rm Edd}$ in Paper II, and here simply note that, while the best estimates for these galaxies' properties are off our grid, they are off by only a very small amount, and any plausible estimate of the errors bars (at least a factor of 2 in both directions, likely more) overlaps the grid extensively.

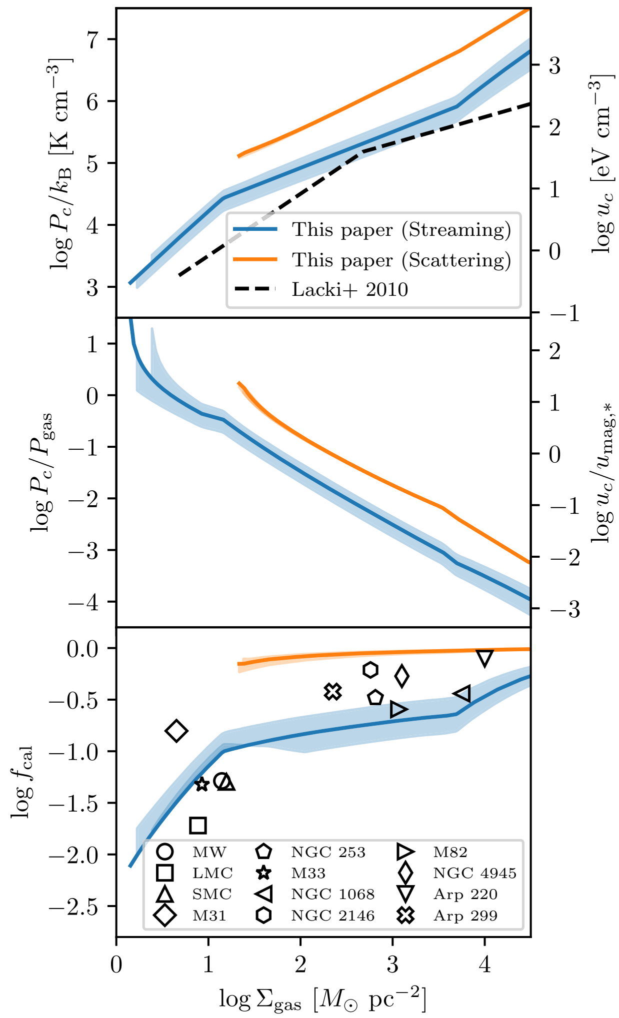

Figure 8. CR pressure and energy density (top panel), ratio of CR pressure to gas pressure (middle panel), and calorimetry fraction (bottom panel) computed as a function of gas surface density, taking the star formation surface density to be the mean value given by the Kennicutt (1998) relation, as illustrated in Fig. 6. We obtain ancillary data properties ($\sigma, f_{\rm gas}, \chi$) along this line by interpolating, using the same procedure as is used to construct the contours in Fig. 5. The blue and orange curves indicate the results for streaming and scattering CR transport models respectively, with the central solid line indicating the result for our fiducial Alfvén Mach number $M_A = 1.5$, and the shaded enclosing region showing the results for $M_A = 1$–2. Note that $f_{\rm Edd}$ generally increases toward lower surface density as one moves along the Kennicutt (1998) relation, and, as a result, for each of the transport models shown there is a minimum surface density below which $f_{\rm Edd}$ is large enough that we can no longer find a hydrostatic solution. The model curves terminate at this surface density.

and illustrated in Fig. 6. In the top panel, we compare our estimated P_c values to those obtained by Lacki et al. (2010). Clearly the results are qualitatively similar, with the 'Scattering' curve somewhat closer to Lacki et al.'s results for our fiducial parameter choices. Note that Lacki et al.'s calculations were empirically constrained to reproduce the observed far-IR–radio correlation and were used to predict γ-ray fluxes and calorimetric fractions from star-forming galaxies across the Kennicutt (1998) relation. A crucial point of this analysis involves not just the ratio of CR to magnetic energy densities, but also the ratio of magnetic energy density to photon energy density, which controls the relative importance of synchrotron and inverse Compton cooling

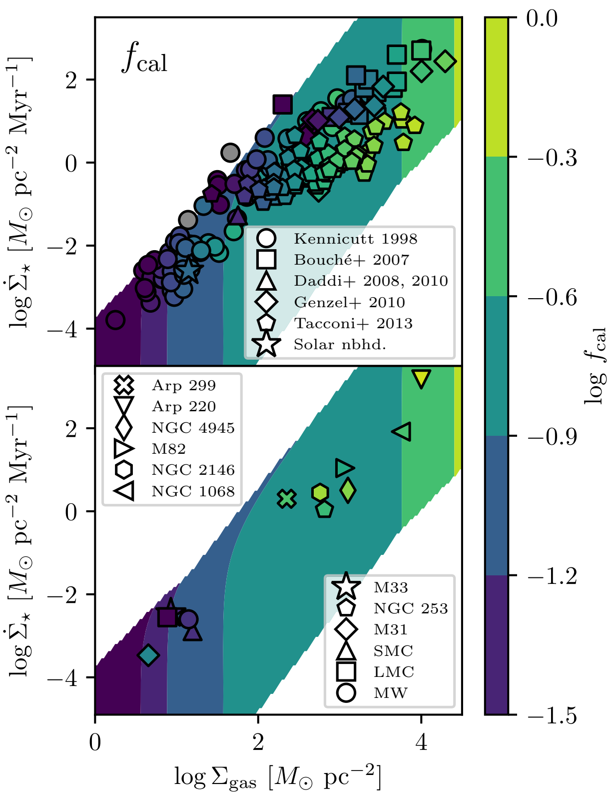

Figure 9. Fraction of CR flux that is absorbed, and thus available to produce γ-rays ($f_{\rm cal}$). In the top panel, we show this quantity estimated for the sample of observed galaxies shown in Fig. 5 (coloured points), computed using the 'Streaming' CR transport model. Grey points mark galaxies whose Eddington ratios place them outside our grid. We also show contours of $\log f_{\rm cal}$, running from −1.5 to 0 in steps of 0.3, interpolated across the plane using the same method as used in Fig. 5. Points that are not covered by contours correspond to combinations of parameters f_g, $f_{\rm Edd}$, $\tau_{\rm abs}$, and $\tau_{\rm stream}$ that are outside our grid of solutions. In the bottom panel, we show the same background contours, but the data points and their colours now indicate gas surface densities, SFRs, and observationally estimated calorimetry fractions for the galaxies listed in Table 4.

for CR electrons. We will explore the predictions of our models for emission from CR electrons in a future paper in this series.

4.3 CR calorimetry

We next examine the fraction $f_{\rm cal}$ of CRs that are lost to pion-producing collisions in Fig. 9. In the top panel, we show predicted calorimetry fractions for the same sample of galaxies plotted in Fig. 5. Here, we see a trend that is generally the opposite of that in Fig. 7: local galaxies tend to have relatively low values of $f_{\rm cal}$, while higher surface density galaxies have higher values. Typical values in galaxies similar to the MW are $\sim 5-10$ per cent, while the fraction rises to ~ 50 per cent in galaxies at the top end of the star-forming sequence.

At first one might be surprised that the difference in calorimetry across the star-forming sequence is as small as it is – after all, the gas surface density increases by ∼4 dex from the LHS to the RHS of Fig. 9, so one might expect a similar level of variation in $f_{\rm cal}$. The main reason that the true variation is not so large, at least in the streaming model, is that the increase in surface density is partly countered by variations in the ionization fraction χ, which change the absorption optical depth as $\tau_{\rm abs} \propto \sqrt{\chi}$ (cf. Table 2); the ionization fraction is lower in the neutral ISM of starbursts than in local spirals due to their much high densities and thus recombination rates (Krumholz et al. 2020). Indeed, Krumholz et al. show that this variation is critical to explaining the observed break in the γ-ray spectra of nearby starbursts above ∼1 TeV. The ionization fraction matters as a direct result of the dependence of the CR streaming speed on the Alfvén Mach number of the ions in a medium where ions and neutrals are decoupled: the lower the ionization fraction, the faster the CR propagation speed and the less time it takes CRs to escape. This effect partially cancels out the increase in gas surface density, going from local spirals to starbursts, which is why $f_{\rm cal}$ rises only by a factor of ∼5–10 across the star-forming sequence.

In the bottom panel of Fig. 9, the background contours show the same predicted theoretical trend as in the upper panel, but now we overplot data points with colours for galaxies with *Fermi*-detected γ-ray emission, for which it is possible to estimate the calorimetry fraction directly. Thus, the data points in the upper panel of Fig. 9 shows *predicted* calorimetry fractions, while those in the lower panel show *measured* (at least approximately) values. We derive our measured values from the observed SFR $\dot{M}_\star$ and γ-ray luminosity L_γ; we take the latter primarily from from Ajello et al. (2020), and the former from a variety of sources in the literature as detailed in Table 4. We estimate the observed calorimetry fraction from these two as

$$f_{\rm cal,obs} = \frac{L_\gamma}{\zeta_{\rm CR} \dot{M}_\star}, \tag{73}$$

where $\zeta_{\rm CR} = 8.3 \times 10^{39}$ erg s^{-1} (M$_\odot$ yr^{-1})$^{-1}$. We derive the conversion factor $\zeta_{\rm CR}$ using from Lacki et al. (2011, their equation 11), and assuming that (1) a fraction $\beta_\gamma = 1/3$ of CRs with energies above the pion production threshold produce neutral pions that decay into γ-rays, (2) a fraction $\beta_\pi = 0.7$ of the energy from these decays goes into γ-rays with energies high enough to be detected by *Fermi* and thus contribute the measured L_γ, and (3) there is one SN per $M_{\star,\rm SN} = 90$ M$_\odot$ of stars formed, each of which explodes with total energy 10^{51} erg, of which a fraction $\eta_c = 0.1$ does into CRs with energies ≥1 GeV. The value of $\zeta_{\rm CR}$ should be regarded as uncertain that the factor of ∼2 level. We list our derived values of $f_{\rm cal,\,obs}$ in Table 4 (uncertain by a factor of ∼2 due to uncertainties in $\zeta_{\rm CR}$), and values predicted by equation (67) for both the streaming and scattering transport models; for the purposes of this computation, we use the surface densities and SFRs listed in the table, and classify galaxies as Local, Intermediate, and Starburst following the same scheme described in Section 4.1. We defer a discussion of the scattering models to Section 4.4, but for now we note that, within the uncertainties in the calorimetric fraction, our streaming model provides reasonable agreement (within ≈0.5 dex) for most galaxies. The largest discrepancies are with the brightest starbursts, where the observationally estimated values of $f_{\rm cal}$ are in the range $\sim 50-80$ per cent, while our model tends to predict values a factor of ∼2 smaller as a result of streaming losses. We can also see this effect in the bottom panel of Fig. 8, where we show our predicted calorimetry fractions along the Kennicutt (1998) relation. Our models provide reasonably good agreement for normal galaxies, but tend to underestimate the calorimetry fractions of starbursts by factors of ∼2.

However, we note that there are a number of confounding factors that should be considered, In addition to the uncertainty on $\xi_{\rm CR}$, our observational estimates of the calorimetry fraction do not account for possible contributions to L_γ from buried active galactic nuclei (AGNs; possibly important in starbursts, though this seems unlikely to be a large effect in our sample, for which star formation

Table 4. Observed and theoretically estimated calorimetry fractions for a sample of *Fermi*-detected galaxies. Columns are as follows: (1) galaxy name; (2) gas surface density; (3) star formation surface density; (4) classification as local (Loc), intermediate (Int), or starburst (SB); (5) SFR; (6) γ-ray luminosity; (7) observationally estimated calorimetric fraction, computed from equation (73); (8) theoretical estimate of $f_{\rm cal}$, computed from equation (67), assuming the streaming CR transport model; (9) same as column (8), but using the scattering transport model; an entry of ... indicates that the estimated parameters for this galaxy place it outside our model grid. Data sources: all γ-ray luminosities L_γ are taken from Ajello et al. (2020), except for those for Arp 220 (from Griffin, Dai & Thompson 2016) and the MW (from Fermi-LAT collaboration 2012). All SFRs for objects classified as Intermediate or Starburst are obtained by converting the total IR luminosity given by Ajello et al. (2020) to an SFR using the conversion given in table 1 of Kennicutt & Evans (2012). Remaining gas and SFR data are from the following sources: MW – gas surface density from McKee et al. (2015), SFR surface density from Fuchs et al. (2009), total SFR from Chomiuk & Povich (2011); LMC and SMC – total gas mass and SFR from Jameson et al. (2016), values per unit area derived by dividing by an area πR_{25}^2, where we take R_{25} from de Vaucouleurs et al. (1991); NGC 224 – total SFR from Rahmani, Lianou & Barmby (2016), gas mass obtained by adding the H I mass from Chemin, Carignan & Foster (2009), and the H_2 mass from Nieten et al. (2006), converted to areal quantities using a radius of 18 kpc from Kennicutt (1998); NGC 253, NGC 1068, NGC 2146, NGC 3035, NGC 4945, Arp 299 – gas and SFR surface densities taken from Liu, Gao & Greve (2015), using gas values for their continuously variable $\alpha_{\rm CO}$ case, and SFR values derived from IR; Arp 220 – Kennicutt (1998), with gas mass and SFR per unit area adjusted to use a conversion factor $\alpha_{\rm CO} = 0.8$ M$_\odot$ pc^{-2} [K km s^{-1}]$^{-1}$, and to a Chabrier (2005) IMF.

Galaxy	$\log \Sigma_{\rm gas}$ (M$_\odot$ pc^{-2})	$\log \dot{\Sigma}_\star$ (M$_\odot$ pc^{-2} Myr^{-1})	Type	$\log \dot{M}_\star$ (M$_\odot$ yr^{-1})	$\log L_\gamma$ (erg s^{-1})	$\log f_{\rm cal,\,obs}$	$\log f_{\rm cal,\,str}$	$\log f_{\rm cal,\,sca}$
Milky Way (MW)	1.15	−2.60	Local	0.28	38.91	− 1.29	− 0.90	−0.10
LMC	0.89	−2.55	Local	−0.70	37.50	− 1.72	− 1.15	...
SMC	1.20	−2.89	Local	−1.48	37.14	− 1.30	− 0.85	−0.09
NGC 224 (M31)	0.65	−3.47	Local	−0.46	38.66	− 0.80	− 1.33	−0.23
NGC 253	2.81	0.04	Intermediate	0.61	40.05	− 0.48	− 0.67	−0.03
NGC 598 (M33)	0.93	−2.46	Local	−0.35	38.25	− 1.32	− 1.11	...
NGC 1068	3.75	1.92	Starburst	1.44	40.92	− 0.44	− 0.77	−0.02
NGC 2146	2.76	0.45	Intermediate	1.24	40.95	− 0.21	− 0.70	−0.03
NGC 3034 (M82)	3.07	1.04	Intermediate	0.94	40.27	− 0.59	− 0.52	−0.02
NGC 4945	3.10	0.51	Intermediate	0.65	40.30	− 0.27	− 0.50	−0.02
Arp 220	4.00	3.18	Starburst	2.38	42.20	− 0.10	− 0.61	−0.01
Arp 299	2.35	0.30	Intermediate	2.05	41.55	− 0.42	− 1.02	−0.06

dominates the bolometric output), and from non-hadronic processes (e.g. bremsstrahlung and inverse Compton emission) or millisecond pulsars (possibly important in galaxies with low SFRs). Similarly, our theoretical models do not account for possible advective escape of CRs that are trapped in the hot phase of the ISM, and never interact with neutral gas. If these are significant, this would reduce $f_{\rm cal}$.

4.4 Dependence on the CR transport model

We now turn to the question of how our results depend on our choice of CR transport model, and on parameters within that model. In Fig. 10, we show our computed CR pressures, ratios of CR to gas pressure, and calorimetric fractions for four different CR transport models: 'Streaming' using $M_A = 1$ and 2, and 'Scattering' also using $M_A = 1$ and 2. All other aspects of the calculation are identical to those discussed previously.

First examining the top two rows of Fig. 10, we see that neither the value of M_A nor the choice of CR transport model has significant qualitative effects on P_c or $P_c/P_{\rm gas}$. For all four cases shown, the CR pressure ranges from $P_c/k_B \sim 10^{3.5}$ K cm^{-3} in sub-MW galaxies to $\sim 10^7$ K cm^{-3} in the brightest starbursts, while the ratio of CR pressure to gas pressure ranges from ~ 1 in sub-MW galaxies to $\sim 10^{-3}$ in starbursts. There are differences at the factor of few level, but nothing larger.

Turning to the third row, we encounter a very different situation. The calorimetric fraction is systematically much lower for the 'Streaming' than for the 'Scattering' transport model. The former has calorimetric fractions of 5 − 10 per cent for MW-like conditions rising to at most $\sim$ 50 per cent in starbursts, while the latter has calorimetric fractions that are at least $\sim$ 50 per cent for MW-like galaxies, rising to nearly 100 per cent in the starburst regime. These differences are also apparent in Fig. 8 and Table 4, where we show results along the Kennicutt (1998) relation, and for a sample of *Fermi*-detected local galaxies, respectively. Clearly the choice of 'Scattering' or 'Streaming' leads to significant changes in the degree of calorimetry. The results also depend substantially on the Alfvén Mach number: even a factor of two change in this quantity produces noticeable changes in $f_{\rm cal}$. These changes are in opposite directions and of different sizes for the two possible models, however: increasing M_A lowers $f_{\rm cal}$ for the 'Streaming' model, while raising it for the 'Scattering' model. Most of the difference between the 'Streaming' and 'Scattering' models can be traced to the comparatively larger value of $\tau_{\rm stream}$ in the streaming model, where the low ion fraction allows fast streaming and thus efficient dissipation.

Based on our analysis in this section, we can see that our conclusions regarding the typical CR pressure and pressure fraction are robust and depend only very weakly on the transport model we adopt. They are ultimately driven by the fact that, regardless of the transport model, lines of constant $P_c/P_{\rm gas}$ correspond to loci of slope close to 2 in the plane of $\Sigma_{\rm gas}$ versus $\dot{\Sigma}_\star$, while the observed relation between these two quantities is not so steep. Our conclusion that the degree of calorimetry increases from low to high surface density galaxies is similarly robust against the transport model we adopt, but the absolute values of the calorimetric fraction are much less so. These appear to depend sensitively on the exact values of the streaming and absorption optical depths, which are functions of the transport model, and are quite sensitive to parameters such as the Alfvén Mach number and (for the scattering model) the CR energy. It is also worth noting that in real galaxies both the 'Streaming' and 'Scattering' transport mechanisms likely co-exist: some CRs are deposited in the neutral phase and experience the former, while some enter the ionized phase and experience the latter; there may also be significant exchange of CRs between the phases. The true degree of calorimetry averaged over the galaxy as a whole is therefore likely

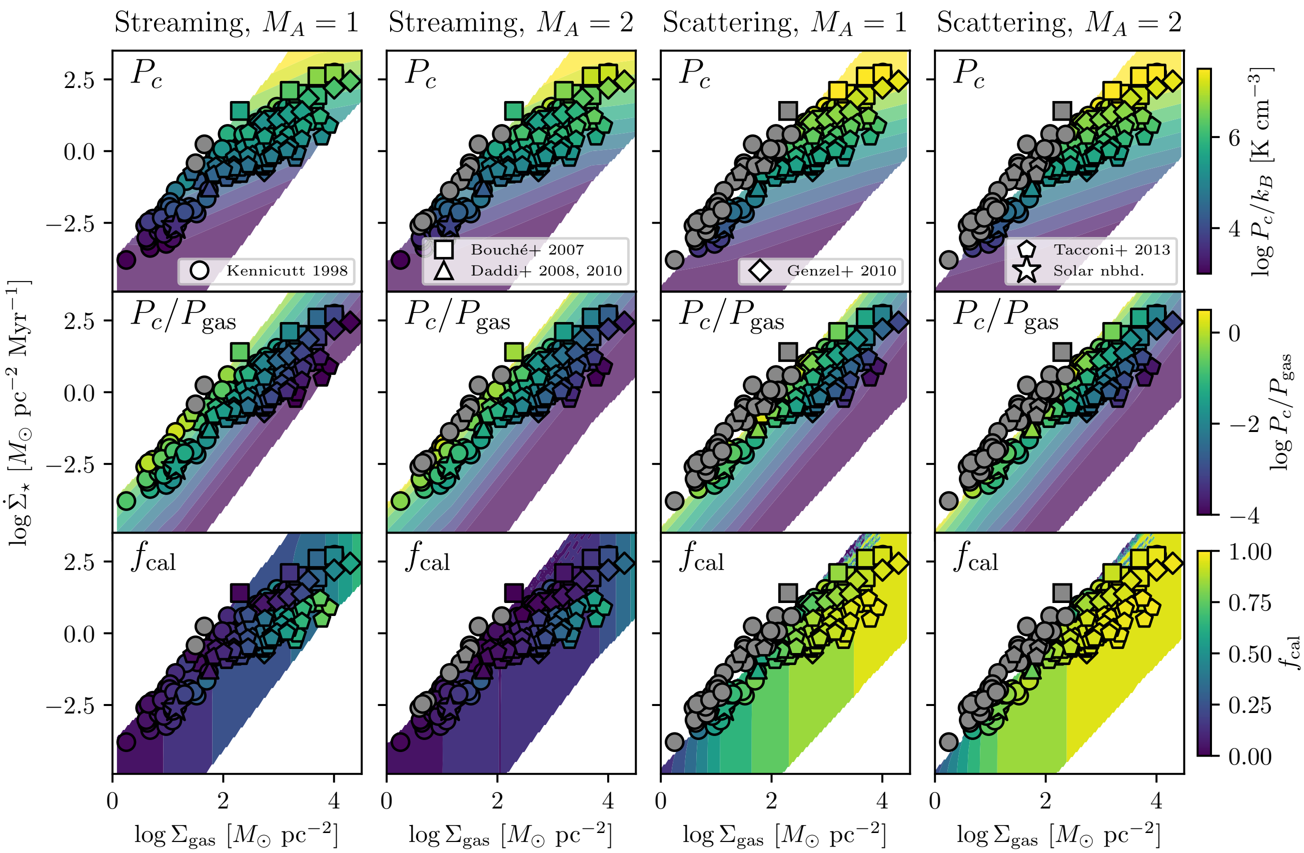

Figure 10. Comparison of results for different CR transport models. The left two columns show the 'Streaming' model, computed using Alfvén Mach numbers $M_A = 1$ and 2, compared to our fiducial choice $M_A = 1.5$; the right two columns show the 'Scattering' model for $M_A = 1$ and 2. The top two rows show the mid-plane CR pressure P_c and ratio of CR pressure to gas pressure $P_c/P_{\rm gas}$, and can be compared directly to Fig. 7; as in that figure, contours are in steps of 0.5 dex, starting from a minimum of $P_c/k_B = 10^3$ K cm^{-3} and $P_c/P_{\rm gas} = 10^{-4}$. The bottom row shows the calorimetric fraction $f_{\rm cal}$, and is comparable to Fig. 9; however, note that, to avoid saturation, we use a different colour scale for $f_{\rm cal}$ here than we do in Fig. 9. Here contours run from 0 to 1 in $f_{\rm cal}$, in steps of 0.1.

to be somewhere in between the two limiting cases that we have explored.

4.5 Caveats and limitations

Our treatment is a semi-analytic, 1D study and, as such, it cannot fully capture the complexity of the real world. In particular, we assume a smoothly evolving ISM density profile while, of course, the real ISMs of galaxies have highly intermittent, multiphase structures. This intermittency has been shown by some of us in previous studies (Krumholz & Thompson 2012, 2013, also see a number of subsequent works by others) to have important implications for indirect radiation pressure feedback where, in particular, gas clumpiness renders photons less efficacious in driving global outflows than one would estimate assuming a smooth ISM density. On the other hand, Thompson & Krumholz (2016) showed, again in the context of radiation pressure feedback, that even for a system that is globally 'sub-Eddington' precisely this ISM intermittency means that photons can launch local outflows from individual, low-surface-density patches of the gas distribution. Ultimately, absent full numerical studies – to which we look forward – in general we cannot be sure about the effect of clumping on CR wind driving. There is, however, a qualitative argument we can adduce that suggests that ISM intermittency may be a less important effect for CRs than photons: the case presented by CRs is qualitatively different to photons because the former move along field lines that thread through both dense clumps and low-density gas, effectively connecting these different phases. This leads us to the qualitative expectation that CRs should be relatively more confined than photons and, therefore, better coupled to the dense gas because of the magnetic field lines that thread throughout the gas. The main exception to this statement will be CRs that are trapped in hot gas that leaves the galaxy at high speed as part of a wind. As discussed above, some fraction of the CRs may not interact with the neutral ISM at all, and thus the main effect of advective escape is likely to be an effective reduction in the $\epsilon_{c,1/2}$ parameter that describes the CR energy per unit mass of stars formed that is injected into the neutral ISM. Note, however, that the very fact that γ-ray emission (that is almost certainly dominantly hadronic) is detected from a number of nearby starbursts means that there is an implicit limit here: at least some CRs have to interact with neutral gas before escaping. This consideration was rendered quantitative by Lacki et al. (2010, 2011) who showed that, granted that CRs are energized by star formation, there are firm, and rather constraining, lower limits on the effective gas density the typical CR 'sees' in escaping a starburst.

5 SUMMARY AND CONCLUSIONS

In this paper, we employ an idealized, slab model of galactic discs to investigate the large-scale, dynamical importance of CRs in supporting the neutral, star-forming ISM across the full sequence of star-forming galaxies, from near-quiescent dwarfs to intense starbursts. Our ultimate goal is to determine under what conditions we expect CRs to make a substantial contribution to the pressure balance of the ISM, as is the case in the MW, and to what extent the role of CR pressure is correlated with the degree of calorimetry in galaxies, that is, the fraction of CRs injected into a galaxy that ultimately produce pions and thence γ-rays. In our model, the vertical column of gas in a galactic disc is maintained in hydrostatic balance by the competition between stellar and gas self-gravity, and a combination of turbulent and CR pressure. CRs generated near the mid-plane travel vertically through the gas column, undergoing losses due to both 'absorption' (i.e. pion-producing *pp*-collisions) and streaming instability as they do so. We show that this system is characterized primarily by three dimensionless numbers: $\tau_{\rm stream}$, $\tau_{\rm abs}$, and $f_{\rm Edd}$ (as given most generally by equations 31, 32, and 36, respectively). These parametrize, respectively, the streaming and absorptive optical depths presented by the gas column to the CRs, and the ratio of the CR momentum flux to the gravitational momentum flux, that is, the CR Eddington ratio.

For any given combination of these three parameters, together with a total gas fraction, we can obtain solutions for the gas density and CR energy density as a function of height, from which we derive our two parameters of interest: the fractional pressure provided by CRs, and the calorimetry fraction, i.e. the fraction of CR flux that is lost to *pp* collisions, and thus becomes available to produce observable γ-ray emission. We show that the CR pressure fraction is primarily determined by $f_{\rm Edd}$, and increases with $f_{\rm Edd}$ from small values for $f_{\rm Edd} \ll 1$ to values of order unity for $f_{\rm Edd} \sim 1$, up to a critical value of $f_{\rm Edd}$ beyond which hydrostatic equilibrium is impossible; we discuss the implications of this finding further in Paper II in this series. By contrast, the degree of calorimetry is controlled primarily by the optical depths, and is insensitive to the Eddington ratio. Calorimetry is maximized when $\tau_{\rm abs} \gg \tau_{\rm stream}$ and $\tau_{\rm abs} \gg 1$.

In order to draw conclusions about observed galaxies, we develop a model to estimate the dimensionless quantities $\tau_{\rm stream}$ (equation 45 or 55, for 'Streaming' or 'Scattering' transport of CRs, respectively), $\tau_{\rm abs}$ (equation 45 or 56), and $f_{\rm Edd}$ (equation 69) from observations, primarily the gas and star formation surface densities of galaxies – the former determines the optical depth and the strength of gravitational confinement (the denominator in $f_{\rm Edd}$), while the latter determines the CR flux per unit area entering the ISM (the numerator in $f_{\rm Edd}$). While these quantities broadly constrain the dimensionless parameters in our model, in detail the mapping between observables and dimensionless quantities depends on the microphysics of CR transport. We therefore consider a range of transport models, corresponding to differing assumptions about the phase of the ISM through which CRs travel, and the mechanism by which they interact with magnetohydrodynamic (MHD) turbulence in the ISM.

Independent of assumptions about transport mode, however, we show that, as the gas column density is dialed upwards, galaxies become increasingly calorimetric and are, therefore, increasingly good γ-ray sources (see Fig. 8 and Table 4; cf. Torres et al. 2004; Thompson et al. 2007; Lacki et al. 2010, 2011; Yoast-Hull et al. 2016; Peretti et al. 2019). CRs are never dynamically important on global scales for gas surface densities exceeding $\sim 10^{2.5}\,{\rm M}_\odot$ pc^{-2} (Figs 7 and 10), and indeed above a gas surface density of $\sim 20\,{\rm M}_\odot$ pc^{-2}, the pressure declines rapidly (see Fig. 8). In the densest starbursts, the ratio of CR to other pressures drops to only $\sim 10^{-3}$–10^{-4}. Conversely, at lower surface gas densities CRs can take on considerable dynamical significance, providing pressure comparable to the gas pressure, but at the same time these galaxies are substantially subcalorimetric. As is implicit in the results of Jubelgas et al. (2008) and as discussed in Socrates et al. (2008), the ultimate factor driving the trend toward smaller dynamical importance for CRs in more dense and intensely star-forming galaxies is rapid pionic losses. As discussed in the context of the radio and gamma-ray emission from star-forming galaxies across the Kennicutt–Schmidt law by Lacki et al. (2010, 2011, see also Thompson & Lacki 2013), the distribution of observed galaxies in the plane of gas and star formation surface densities guarantees that high gas surface density systems will have the smallest overall CR pressure relative to that required for hydrostatic equilibrium. At high gas surface densities where pion production is the dominant loss mechanism for CRs, the CR pressure scales with SFR and gas surface density as

$$P_{\rm CR} \propto \frac{\dot{E}_{\rm CR} t_{\rm col}}{\rm Volume} \propto \frac{\rm SFR}{\pi R^2}\frac{t_{\rm col}}{h} \propto \frac{\dot{\Sigma}_\star}{\Sigma_{\rm gas}} \simeq 1\times 10^5\ {\rm K\ cm^{-3}}\ \dot{\Sigma}_{\star,-1}\ \Sigma_{\rm gas,2}^{-1} \qquad (74)$$

where SFR is the total star formation rate, $\dot{E}_{\rm CR}$ is the total CR energy injection rate, $t_{\rm col}$ is the pion loss timescale (equations 11 and 13), and the approximate equality in the second line provides a numerical value scaled to $\dot{\Sigma}_{\star,-1} = \dot{\Sigma}_\star/(0.1\,{\rm M}_\odot\ {\rm pc}^{-2}\ {\rm Myr}^{-1})$ and $\Sigma_{\rm gas,2} = \Sigma_{\rm gas}/(100\,{\rm M}_\odot\ {\rm pc}^{-2})$. By contrast, the self-gravitational pressure of a galactic disc scales as $P_* \propto \Sigma_{\rm gas}^2$, so that

$$P_{\rm CR}/P_* \propto \dot{\Sigma}_\star/\Sigma_{\rm gas}^3.$$

Thus, maintaining constant $P_{\rm CR}/P_*$ would require that the SFR surface density increase as the cube of the gas surface density. This corresponds to a Kennicutt–Schmidt relation with index of 3, whereas the observed index of the relation is much shallower and ranges from $\approx$1 to 2. The decline in the dynamical importance of CRs at high surface density follows directly from this. At the same time, galaxies with higher gas surface densities do have higher absorption optical depths, and thus are more calorimetric. This combination drives the anticorrelation between CR dynamical importance and calorimetry in galaxies (Lacki et al. 2011; Thompson & Lacki 2013).

Finally, we remark that the model we have presented here has obvious further applications. We have already mentioned one of these, which is the subject of Paper II: launching of CR-driven cool galactic winds. A further follow-up is to combine our results here with those of Crocker et al. (2018a), who develop a similar plane-parallel atmosphere model for radiation transport out of galactic discs. Combining these models will yield fully self-consistent predictions for the run of gas density, CR energy density, and radiation energy, and thus for the synchrotron and inverse Compton emission produced by leptonic CRs. This will be the subject of future work.

ACKNOWLEDGEMENTS

This research was funded by the Australian Government through the Australian Research Council, awards FT180100375 (MRK) and DP190101258 (RMC, MRK, and TAT). RMC gratefully acknowledges conversations with Felix Aharonian, Geoff Bicknell, Yuval Birnboim, Luke Drury, Alex Lazarian, Chris McKee, Christoph Pfrommer, Heinz Völk, and Siyao Xu. MRK and TAT acknowledge support from the Simons Foundation through the Simons Symposium Series 'Galactic Superwinds: Beyond Phenomenology', during which they collaborated on this work. MRK carried out part of this work during a sabbatical funded by an Humboldt Research Fellowship. TAT thanks Brian Lacki, Eliot Quataert, Ben Buckman, and Tim Linden for discussions and collaboration. TAT is supported in part by National Science Foundation grant number 1516967 and

NASA ATP 80NSSC18K0526. We thank the anonymous referee for a constructive and useful report.

DATA AVAILABILITY STATEMENT

No new data were generated or analysed in support of this research.

REFERENCES

Abdo A. A. et al., 2010, ApJ, 709, L152
Acero F. et al., 2009, Science, 326, 1080
Ajello M., Di Mauro M., Paliya V. S., Garrappa S., 2020, ApJ, 894, 88
Andrews B. H., Thompson T. A., 2011, ApJ, 727, 97
Badhwar G. D., Stephens S. A., 1977, ApJ, 212, 494
Beck R., 2015, A&AR, 24, 4
Bell A. R., 1978, MNRAS, 182, 147
Blasi P., 2019, Galaxies, 7, 64
Booth C. M., Agertz O., Kravtsov A. V., Gnedin N. Y., 2013, ApJ, 777, L16
Bouché N. et al., 2007, ApJ, 671, 303
Boulares A., Cox D. P., 1990, ApJ, 365, 544
Breitschwerdt D., McKenzie J. F., Voelk H. J., 1991, A&A, 245, 79
Breitschwerdt D., McKenzie J. F., Voelk H. J., 1993, A&A, 269, 54
Buck T., Pfrommer C., Pakmor R., Grand R. J., Springel V., 2019, MNRAS, 497, 1712
Caldú-Primo A., Schruba A., Walter F., Leroy A., Bolatto A. D., Vogel S., 2015, AJ, 149, 76
Chabrier G., 2005, The Initial Mass Function 50 Years Later, Vol. 327. Springer, Dordrecht, p. 41
Chan T. K., Kereš D., Hopkins P. F., Quataert E., Su K.-Y., Hayward C. C., Faucher-Giguère C.-A., 2019, MNRAS, 488, 3716
Chemin L., Carignan C., Foster T., 2009, ApJ, 705, 1395–1415
Chevalier R. A., Fransson C., 1984, ApJ, 279, L43
Chomiuk L., Povich M. S., 2011, AJ, 142, 197
Condon J. J., 1992, ARA&A, 30, 575
Crocker R. M., 2012, MNRAS, 423, 3512
Crocker R. M., Jones D. I., Aharonian F., Law C. J., Melia F., Ott J., 2011, MNRAS, 411, L11
Crocker R. M., Krumholz M. R., Thompson T. A., Clutterbuck J., 2018, MNRAS, 478, 81
Crocker R. M., Krumholz M. R., Thompson T. A., Baumgardt H., Mackey D., 2018, MNRAS, 481, 4895
Crocker R. M., Krumholz M. R., Thompson T. A., 2020, MNRAS, preprint (arXiv:2006.15821) (Paper II)
Daddi E., Dannerbauer H., Elbaz D., Dickinson M., Morrison G., Stern D., Ravindranath S., 2008, ApJ, 673, L21
Daddi E. et al., 2010a, ApJ, 713, 686
Davis S. W., Jiang Y. F., Stone J. M., Murray N., 2014, ApJ, 796, 107
de Vaucouleurs G., de Vaucouleurs A., Corwin H. G., Jr, Buta R., Patural G., Fouque P., 1991, Third References Catalogue of Bright Galaxies, Springer, New York, NY, USA
Dekel A., Sarkar K. C., Jiang F., Bournaud F., Krumholz M. R., Ceverino D., Primack J., 2019, MNRAS, 4, 4753
Domingo-Santamaría E., Torres D. F., 2005, A&A, 444, 403
Drury L. O., Markiewicz W. J., Voelk H. J., 1989, A&A, 225, 179
Everett J. E., Zweibel E. G., Benjamin R. A., McCammon D., Rocks L., Gallagher J. S. III, 2008, ApJ, 674, 258
Farber R., Ruszkowski M., Yang H.-Y. K., Zweibel E. G., 2018, ApJ, 856, 112
Farmer A. J., Goldreich P., 2004, ApJ, 604, 671
Faucher-Giguère C. A., Quataert E., Hopkins P. F., 2013, MNRAS, 433, 1970
Federrath C., 2016, J. Plasma Phys., 82, 535820601
Federrath C., Schober J., Bovino S., Schleicher D. R. G., 2014, ApJ, 797, L19
Fermi-LAT collaboration et al., 2012, ApJ, 755, 164
Fermi-LAT collaboration et al., 2020, ApJS, 247, 33
Fuchs B., Jahreiß H., Flynn C., 2009, AJ, 137, 266
Funk S., 2015, Annu. Rev. Nucl. Part. Sci., 65, 245
Genzel R. et al., 2010, MNRAS, 407, 2091
Gerke J. R., Kochanek C. S., Stanek K. Z., 2015, MNRAS, 450, 3289
Ghosh A., Ptuskin V. S., 1983, Ap&SS, 92, 37
Ginzburg V. L., Syrovatskii S. I., 1964, The Origin of Cosmic Rays. Macmillan, New York
Griffin R. D., Dai X., Thompson T. A., 2016, ApJ, 823, L17
Hanasz M., Lesch H., Naab T., Gawryszczak A., Kowalik K., Wóltański D., 2013, ApJ, 777, L38
Hayward C. C., Hopkins P. F., 2017, MNRAS, 465, 1682
Heintz E., Zweibel E. G., 2018, ApJ, 860, 97
Heintz E., Bustard C., Zweibel E. G., 2020, ApJ, 891, 157
Hillas A. M., 2005, JPGNP, 31, 95
Ianjamasimanana R., de Blok W. J. G., Walter F., Heald G. H., Caldú-Primo A., Jarrett T. H., 2015, AJ, 150, 47
Ipavich F. M., 1975, ApJ, 196, 107
Jameson K. E. et al., 2016, ApJ, 825, 12
Jokipii J. R., 1971, Rev. Geophys. Space Phys., 9, 27
Jokipii J. R., 1976, ApJ, 208, 900
Jubelgas M., Springel V., Enßlin T., Pfrommer C., 2008, A&A, 481, 33
Kafexhiu E., Aharonian F., Taylor A. M., Vila G. S., 2014, Phys. Rev. D, 90, 123014
Kennicutt R. C., Jr, 1998, ApJ, 498, 541
Kennicutt R. C., Jr., Evans N. J. E. II., 2012, ARA&A, 50, 531
Ko C. M., Dougherty M. K., McKenzie J. F., 1991, A&A, 241, 62
Krumholz M. R., 2015, preprint (arXiv:1511.03457)
Krumholz M. R., Burkhart B., 2016, MNRAS, 458, 1671
Krumholz M. R., Tan J. C., 2007, ApJ, 654, 304
Krumholz M. R., Thompson T. A., 2012, ApJ, 760, 155
Krumholz M. R., Thompson T. A., 2013, MNRAS, 434, 2329
Krumholz M. R., Dekel A., McKee C. F., 2012, ApJ, 745, 69
Krumholz M. R., Burkhart B., Forbes J. C., Crocker R. M., 2018, MNRAS, 477, 2716
Krumholz M. R., Crocker R. M., Xu S., Lazarian A., Rosevear M. T., Bedwell-Wilson J., 2020, MNRAS, 493, 2817
Lacki B. C., 2013, preprint (arXiv:1308.5232)
Lacki B. C., Beck R., 2013, MNRAS, 430, 3171
Lacki B. C., Thompson T. A., Quataert E., 2010, ApJ, 717, 1
Lacki B. C., Thompson T. A., Quataert E., Loeb A., Waxman E., 2011, ApJ, 734, 107
Leroy A. K. et al., 2017, ApJ, 846, 71
Liu L., Gao Y., Greve T. R., 2015, ApJ, 805, 31
Martin P., 2014, A&A, 564, A61
McKee C. F., Parravano A., Hollenbach D. J., 2015, ApJ, 814, 13
McKenzie J. F., Voelk H. J., 1982, A&A, 116, 191
Nieten Ch., Neininger N., Guélin M., Ungerechts H., Lucas R., Berkhuijsen E. M., Beck R., Wielebinski R., 2006, A&A, 453, 459
Nomoto K., Tominaga N., Umeda H., Kobayashi C., Maeda K., 2006, Nucl. Phys. A, 777, 424
Ostriker E. C., Shetty R., 2011, ApJ, 731, 41
Ostriker E. C., Stone J. M., Gammie C. F., 2001, ApJ, 546, 980
Paglione T. A. D., Abrahams R. D., 2012, ApJ, 755, 106
Pakmor R., Pfrommer C., Simpson C. M., Springel V., 2016, ApJ, 824, L30
Parker E. N., 1966, ApJ, 145, 811
Pejcha O., Thompson T. A., 2015, ApJ, 801, 90
Peng F.-K., Wang X.-Y., Liu R.-Y., Tang Q.-W., Wang J.-F., 2016, ApJ, 821, L20
Peretti E., Blasi P., Aharonian F., Morlino G., 2019, MNRAS, 487, 168
Persic M., Rephaeli Y., Arieli Y., 2008, A&A, 486, 143
Pfrommer C., Pakmor R., Simpson C. M., Springel V., 2017, ApJ, 847, L13
Ptuskin V. S., 2001, Space Sci. Rev., 99, 281
Ptuskin V. S., Voelk H. J., Zirakashvili V. N., Breitschwerdt D., 1997, A&A, 321, 434
Ptuskin V. S., Moskalenko I. V., Jones F. C., Strong A. W., Zirakashvili V. N., 2006, ApJ, 642, 902
Rahmani S., Lianou S., Barmby P., 2016, MNRAS, 456, 4128
Raskutti S., Ostriker E. C., Skinner M. A., 2016, ApJ, 829, 130
Raskutti S., Ostriker E. C., Skinner M. A., 2016, ApJ, 850, 112

Recchia S., Blasi P., Morlino G., 2016, MNRAS, 462, 4227
Recchia S., Blasi P., Morlino G., 2017, MNRAS, 470, 865
Rodrigues L. F. S., Sarson G. R., Shukurov A., Bushby P. J., Fletcher A., 2016, ApJ, 816, 1
Rojas-Bravo C., Araya M., 2016, MNRAS, 463, 1068
Ruszkowski M., Yang H.-Y. K., Zweibel E., 2017, ApJ, 834, 208
Ryu D., Kim J., Hong S. S., Jones T. W., 2020, ApJ, 589, 338
Salem M., Bryan G. L., 2014, MNRAS, 437, 3312
Salem M., Bryan G. L., Corlies L., 2016, MNRAS, 456, 582
Samui S., Subramanian K., Srianand R., 2010, MNRAS, 402, 2778
Simpson C. M., Pakmor R., Marinacci F., Pfrommer C., Springel V., Glover S. C. O., Clark P. C., Smith R. J., 2016, ApJ, 827, L29
Skilling J., 1971, ApJ, 170, 265
Skinner M. A., Ostriker E. C., 2015, ApJ, 809, 187
Socrates A., Davis S. W., Ramirez-Ruiz E., 2008, ApJ, 687, 202
Stilp A. M., Dalcanton J. J., Warren S. R., Skillman E., Ott J., Koribalski B., 2013, ApJ, 765, 136
Strong A. W., Porter T. A., Digel S. W., Jóhannesson G., Martin P., Moskalenko I. V., Murphy E. J., Orlando E., 2010, ApJ, 722, L58
Suchkov A., Allen R. J., Heckman T., 1993, ApJ, 413, 542
Sudoh T., Totani T., Kawanaka N., 2018, PASJ, 70, 49
Tacconi L. J. et al., 2013, ApJ, 768, 74
Tennekes H., Lumley J. L., 1972, First Course in Turbulence. MIT Press, Cambridge
Thompson T. A., Krumholz M. R., 2016, MNRAS, 455, 334
Thompson T. A., Lacki B. C., 2013, Cosmic Rays in Star-forming Environments. Springer-Verlag, Berlin Heidelberg, p. 283
Thompson T. A., Quataert E., Murray N., 2005, ApJ, 630, 167
Thompson T. A., Quataert E., Waxman E., Murray N., Martin C. L., 2006, ApJ, 645, 186
Thompson T. A., Quataert E., Waxman E., 2007, ApJ, 654, 219
Torres D. F., Reimer O., Domingo-Santamaría E., Digel S. W., 2004, ApJ, 607, L99
Tsang B. T. H., Milosavljević M., 2015, MNRAS, 478, 4142
Tsang B. T. H., Milosavljević M., 2015, MNRAS, 453, 1108
Uhlig M., Pfrommer C., Sharma M., Nath B. B., Enßlin T. A., Springel V., 2012, MNRAS, 423, 2374
Utomo D. et al., 2018, ApJ, 861, L18
VERITAS Collaboration et al., 2009, Nature, 462, 770
Völk H. J., Aharonian F. A., Breitschwerdt D., 1996, Space Sci. Rev., 75, 279
Wadepuhl M., Springel V., 2011, MNRAS, 410, 1975
Wentzel D. G., 1974, ARA&A, 12, 71
Wibking B. D., Thompson T. A., Krumholz M. R., 2018, MNRAS, 477, 4665
Wiener J., Zweibel E. G., Oh S. P., 2013, ApJ, 767, 87
Wiener J., Pfrommer C., Oh S. P., 2017, MNRAS, 467, 906
Wolfire M. G., McKee C. F., Hollenbach D., Tielens A. G. G. M., 2003, ApJ, 587, 278
Xi S.-Q., Liu R.-Y., Zhang H.-M., Wang X.-Y., 2020, ApJ, 901, 158
Xu S., Lazarian A., 2017, New J. Phys., 19, 065005
Yoast-Hull T. M., Murray N., 2019, MNRAS, 484, 3665
Yoast-Hull T. M., Gallagher J. S., Zweibel E. G., 2016, MNRAS, 457, L29
Zirakashvili V. N., Völk H. J., 2006, ApJ, 636, 140
Zirakashvili V. N., Breitschwerdt D., Ptuskin V. S., Voelk H. J., 1996, A&A, 311, 113
Zweibel E. G., 2017, Phys. Plasmas, 24, 055402

APPENDIX A: ON THE STREAMING SPEED OF ∼GEV CRS IN LOCAL SPIRAL AND DWARF GALAXIES

In the main text and in Paper II, the form of the diffusion coefficient we adopt in the case of streaming and for the dynamically dominant ∼GeV CRs assumes that the streaming speed is identical to the ion Alfvén speed. We showed that this is an accurate approximation for starburst environments in Krumholz et al. (2020). Here, we show that it remains a tolerably accurate assumption down to the much lower gas densities typical of the neutral ISM in local spirals and dwarfs. Moreover, as we also show, the assumption remains valid irrespective of the identity of the dominant ionized species (in particular, whether the dominant species is C^+ at $\chi \sim 10^{-4}$ in starbursts or H^+ at $\chi \sim 10^{-2}$ in MW conditions).

First, we recapitulate the results for starburst-like ISM conditions derived in Krumholz et al. (2020). Make the empirically motivated assumption that the CRs fall into a power-law distribution with respect to Lorentz factor γ, $\mathrm{d}n_{\rm CR}/\mathrm{d}\gamma \propto \gamma^{-p}$. Then we can write $n_{\rm CR}(>\gamma) = C\gamma^{-p+1}$; for the MW near the Solar Circle, $C = C_{\rm MW} \approx 2\times 10^{-10}$ cm^{-3} and $p \approx 2.6$ (Wentzel 1974; Farmer & Goldreich 2004). Adopting this functional form for $n_{\rm CR}(>\gamma)$, Krumholz et al. (2020) show that the growth rate of the streaming instability balances the rate at which it damps due to ion-neutral drag if the CR streaming velocity relative to the ion Alfvén speed obeys

$$\begin{aligned}\frac{v_s}{v_{\rm A,i}} - 1 &= \frac{\gamma_{\rm d}\chi\mathcal{M}_{\rm A}c}{4Ceu_{\rm LA}\mu_{\rm i}\gamma^{-p+1}}\sqrt{\frac{m_{\rm H}m^2\mu_{\rm H}^3 n_{\rm H}^3}{\pi}}\\ &\simeq 2.3\times 10^{-3}\frac{E_{\rm CR,0}^{p-1} n_{\rm H,3}^{3/2}\chi_{-4}\mathcal{M}_{\rm A}}{C_3 u_{\rm LA,1}},\end{aligned}\qquad\text{(A1)}$$

where $\gamma_{\rm d}$ is the ion-neutral drag coefficient, μ_i is the mean particle mass of the ions in units of amu, $u_{\rm LA}$ is the turbulent velocity of Alfvénic modes at the injection scale of the turbulence (which we can, with good accuracy, take to be identical to σ), $C_3 = C/1000C_{\rm MW} = C/2\times 10^{-7}$ cm^{-3}, and the numerical evaluation is for CR protons ($m = m_{\rm H}$) and, in the first instance, a population of ions dominated by C^+ ($\mu_{\rm i} = 12$).

Note from equation (A1) that, while the CR energy density is significantly in excess of MW values, we are guaranteed that the streaming velocity will be very close to $v_{\rm A,\,i}$, the ion Alfvén speed. For MW conditions, we need to renormalize equation (A1) and we now take the dominant ionized species to be protons ($\mu_i \to 1$) and assume a much lower CR number density $C \sim C_{\rm MW}$ and gas number density $n_{\rm H} \sim 1$ cm^{-3} (the mean for MW mid-plane) and a much higher ionization fraction $\chi \sim 10^{-2}$ (Wolfire et al. 2003), in which case we find:

$$\frac{v_s}{v_{\rm A,i}} - 1 \simeq 0.086\frac{E_{\rm CR,0}^{p-1} n_{\rm H,0}^{3/2}\chi_{-2}\mathcal{M}_{\rm A}}{C_0 u_{\rm LA,1}},\qquad\text{(A2)}$$

where $C_0 \equiv C/C_{\rm MW} = C/2\times 10^{-10}$ cm^{-3} and $n_{\rm H,\,0} \equiv n_{\rm H}/(1$ cm$^{-3})$. Comparing equations (A1) and (A2), one can see that, normalizing to MW-like conditions and, in particular, accounting for the increase in ion neutral drag when going from C^+ to mostly from protons, then the streaming speed goes up from 0.2 per cent above the Alfvén ion speed to ∼10 per cent above the Alfvén ion for ∼GeV CRs. For dwarfs, sub-MW CR energy densities will push the streaming speed to be still larger relative to the ion Alfvén speed, but this is somewhat ameliorated by the corresponding decline in neutral ISM number density; we estimate that for the most extreme dwarfs in the parameter space one might reach a streaming speed ∼50 per cent in excess of $v_{\rm A,\,i}$. Altogether, we take these calculations to indicate that setting $v_s = v_{\rm A,\,i}$ for GeV CRs is a well-justified assumption over the entire Kennicutt–Schmidt plane.

APPENDIX B: PARKER STABILITY

In this appendix, we consider the possible impact of Parker (1966) stability on our conclusions. Since Parker's initial calculation, a number of authors have extended the analysis include the effects of CR diffusion and streaming (Ryu et al. 2003; Rodrigues et al. 2016; Heintz & Zweibel 2018; Heintz, Bustard & Zweibel 2020), which are generally destabilizing. The basic conclusion of this analysis is that galactic discs across a wide range of parameter space are generally subject to Parker instability. We therefore expect that many of our models will be Parker unstable. However, this seems unlikely to modify our conclusions substantively, for the following reason: the effect of the instability is to drive turbulent motions, and to increase CR flux compared to our estimates, that is, to allow CRs to propagate through the gas more rapidly than our laminar calculation suggests. The effect of turbulence is already included empirically in our models, since we simply rely on observed gas velocity dispersions, and thus is not important. In principle, however, the increased flux made possible by the instability could lead to lower CR pressures near the mid-plane, which would increase the stability of the system against self-gravity.

However, there is an important limit to the amount by which Parker instability might contribute to the flux, which is that the *mechanism* by which Parker instability increases the flux is through convective motions of the gas. When the instability occurs, buoyant magnetic field lines and their associated CRs rise in arches, while gas falls between the arches into valleys. Because the transport is convective, the maximum CR flux that results from Parker instability is ultimately limited by the speed of the rising arches that carry the CRs: $F_{c,\mathrm{P}} < \sigma u_c$; the true transport rate is certainly smaller than this, since this is the flux that would apply if the gas were moving uniformly at speed σ. In terms of our dimensionless variables, we can therefore write the ratio of the Parker instability-driven flux $F_{c,\mathrm{P}}$ to the diffusive flux F_c (equation 14) as

$$\frac{F_{c,\mathrm{P}}}{F_c} < \frac{3}{K_* f_c}, \tag{B1}$$

where f_c is the dimensionless CR propagation speed defined by equation (64). This ratio takes on its maximum value as $\xi \to \infty$, where it is

$$\frac{F_{c,\mathrm{P}}}{F_c} < \frac{3}{4K_* \tau_{\mathrm{stream}}} = \frac{3\sigma}{4v_s} = \frac{3}{2\sqrt{2}} M_A \left(\sqrt{\chi}, 1\right), \tag{B2}$$

where the first term in parentheses applies for the streaming propagation model, and the second for the scattering or constant κ_* models. Thus, we see that, unless $\mathcal{M}_A \gg 1$ (and $\gg 1/\sqrt{\chi}$ for the streaming transport model), CR transport via Parker instability is always comparable to or smaller than the flux we have already included in our models. We therefore conclude the Parker instability cannot significantly alter our conclusions.

This paper has been typeset from a TEX/LATEX file prepared by the author.